

Eglantine Boulard
eglantine.boulard@sorbonne-universite.fr

Institut de minéralogie,
de physique des matériaux
et de cosmochimie (IMPMC)

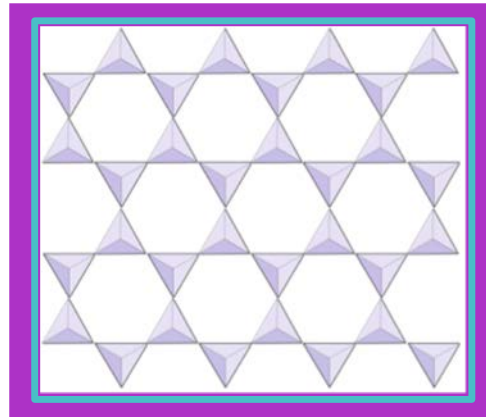
Mantle Mineralogy

- Experimental Petrology and Mineral Physics
- Mineralogy of the mantle and subducting slabs
- Case Study: Deep Carbon Cycle

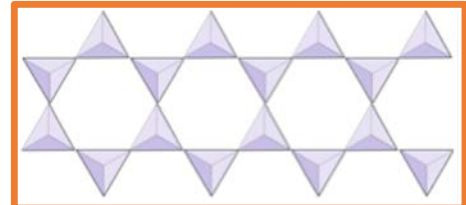


Mineralogy of the mantle and subducting slabs

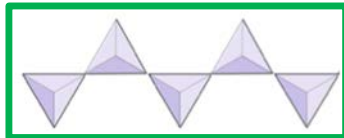
Mineralogy of the Crust



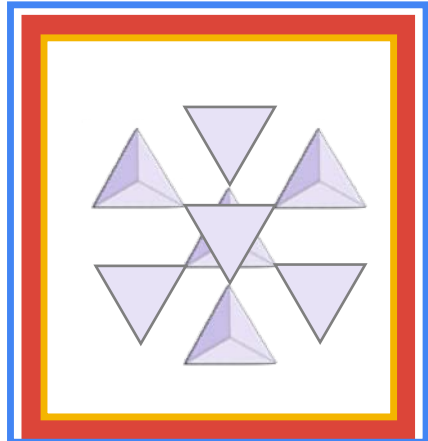
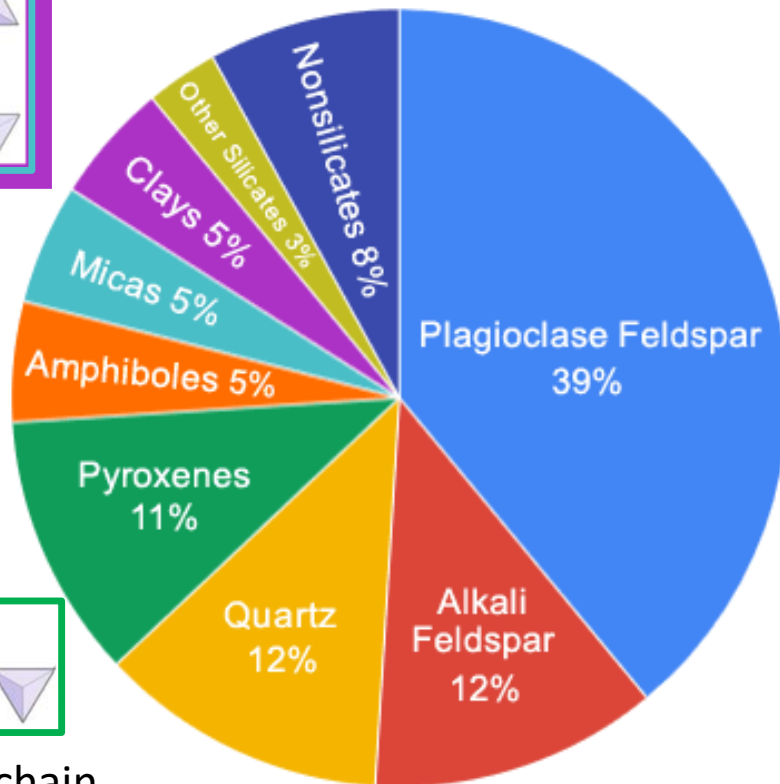
Phyllosilicates



Inosilicates double chains



Inosilicates single chain



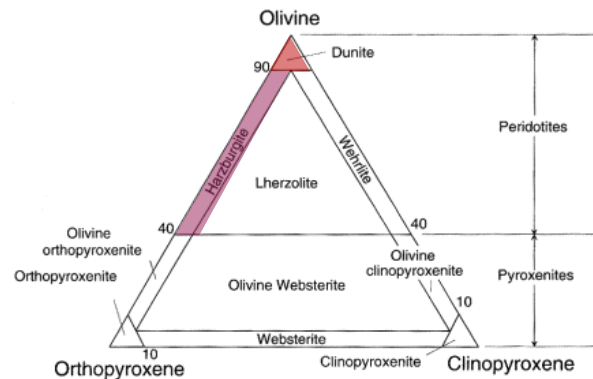
Tectosilicates

Mantle Pyrolite Model

Mix of
Peridotite (Dunite/Harzburgite) + tholeitic Basalt

Ringwood, JGR, 1962

PYroxene OLIvine



	Pyrolite ^a	Harzburgite ^a	MORB ^b
SiO ₂	38.9	36.4	52.2
Al ₂ O ₃	2.2	0.7	10.2
CaO	3.1	0.9	14.8
MgO	50.0	56.6	15.8
FeO	5.8	5.4	7.0
Mg/Si	1.29	1.55	0.30
Fe/Si	0.15	0.15	0.13
Ca/Si	0.08	0.02	0.28
Al/Si	0.11	0.04	0.39

Where these elements reside dictates elastic and transport properties

But is the Mantle Really Pyrolytic?

Table 13.1 | Estimates of average composition of the mantle

Oxide	(1)	(2)	(3)	(4)	(5)
SiO_2	45.23	47.9	44.58	47.3	45.1
Al_2O_3	4.19	3.9	2.43	4.1	3.9
MgO	38.39	34.1	41.18	37.9	38.1
CaO	3.36	3.2	2.08	2.8	3.1
FeO	7.82	8.9	8.27	6.8	7.9
TiO_2	—	0.20	0.15	0.2	0.2
Cr_2O_3	—	0.9	0.41	0.2	0.3
Na_2O	—	0.25	0.34	0.5	0.4
K_2O	—	—	0.11	0.2	(0.13)

- (1) Jacobsen and others (1984): extrapolation of ultramafic and chondritic trends.
- (2) Morgan and Anders (1980): cosmochemical model.
- (3) Maaløe and Steel (1980): extrapolation of lherzolite trend.
- (4) 20 percent eclogite, 80 percent garnet lherzolite (Anderson, 1980).
- (5) Ringwood and Kesson (1976, Table 7): pyrolite adjusted to have chondritic $\text{CaO}/\text{Al}_2\text{O}_3$ ratio and Ringwood (1966) for K_2O .

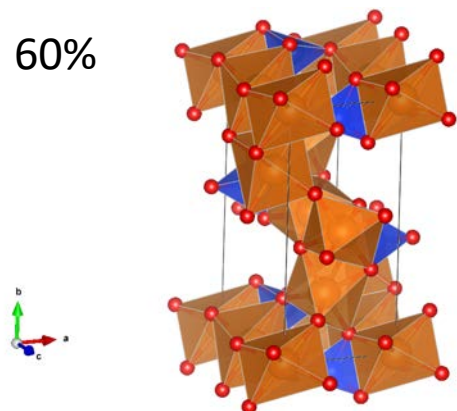
Mg/Si	Fe/Si	Ca/Si	Al/Si
0.85	0.17	0.07	0.09
0.71	0.18	0.06	0.08
0.92	0.18	0.04	0.05
0.80	0.14	0.05	0.08
0.84	0.17	0.07	0.08

Mantle Mineralogy in Pyrolite Model

Olivine $(\text{Fe}, \text{Mg})_2\text{SiO}_4$



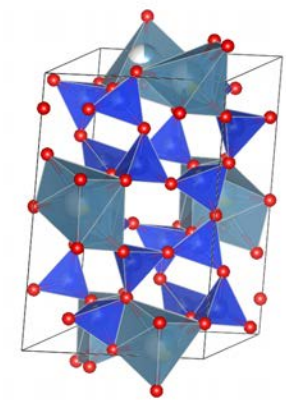
60%



Plagioclase $(\text{Ca}[\text{Al}_2\text{Si}_2\text{O}_8]-\text{Na}[\text{AlSi}_3\text{O}_8])$



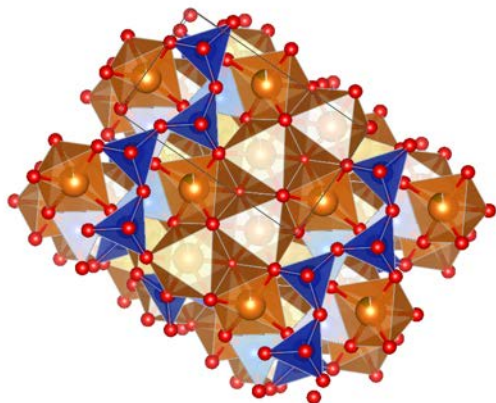
10%



Orthopyroxene $(\text{Fe}, \text{Mg})_2\text{Si}_2\text{O}_6$



b
c
a

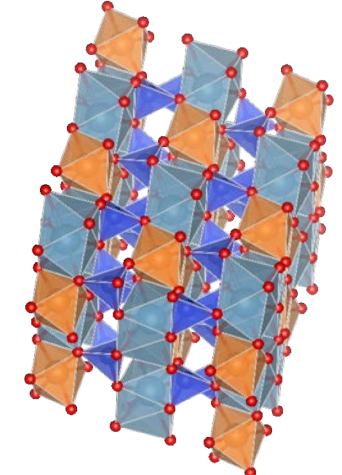


Clinopyroxene $(\text{Ca}, \text{Fe}, \text{Mg})_2\text{Si}_2\text{O}_6$



25%
Les Houches 2022

a
b
c



Mantle Mineralogy in Pyrolite Model

Olivine $(\text{Fe}, \text{Mg})_2\text{SiO}_4$

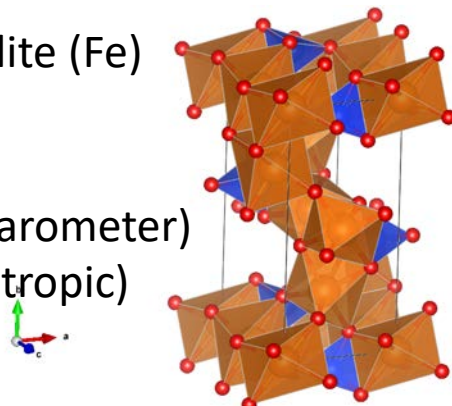
Forsterite (Mg), Fayalite (Fe)

Nesosilicate

Fe : 8-12%

Can uptake Ca (geobarometer)

Orthorhombic (anisotropic)

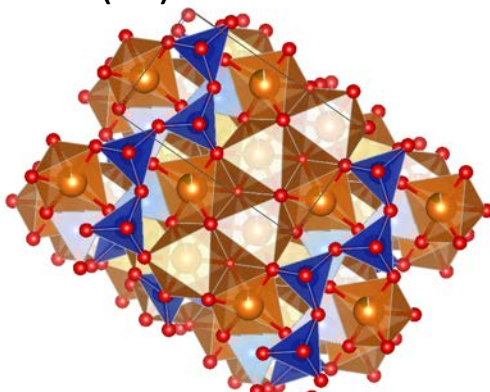


Orthopyroxene $(\text{Fe}, \text{Mg})_2\text{Si}_2\text{O}_6$

Enstatite (Mg), Ferrosilite (Fe)

Inosilicate

orthorhombic



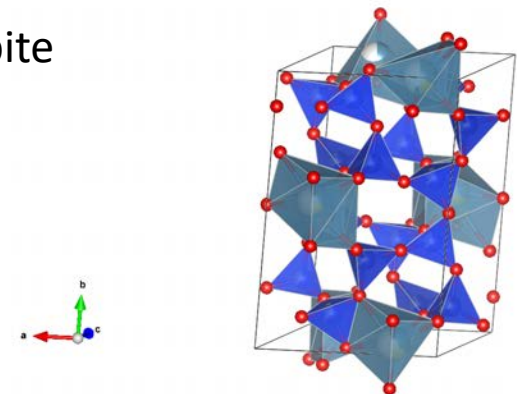
Fe/Mg ratio + opx/cpx ration = geobarometer

Plagioclase $\text{Ca}[\text{Al}_2\text{Si}_2\text{O}_8]-\text{Na}[\text{AlSi}_3\text{O}_8]$

Anorthite - albite

Tectosilicate

monoclinic

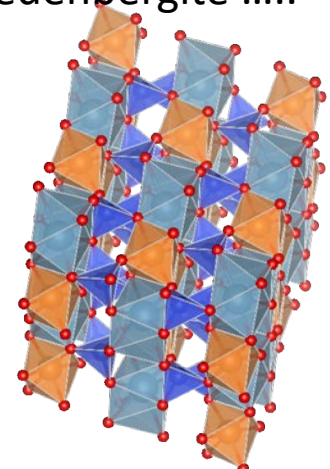


Clinopyroxene $(\text{Ca}, \text{Fe}, \text{Mg})_2\text{Si}_2\text{O}_6$

Pigeonite, Diopside, hedenbergite

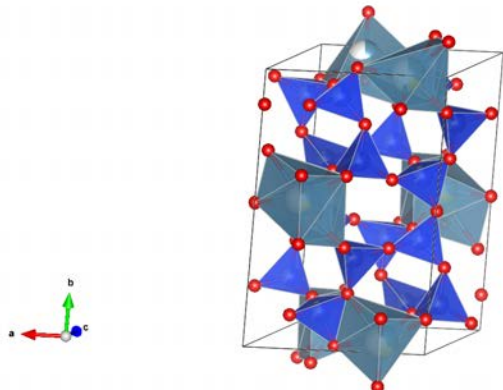
Inosilicate

orthorhombic

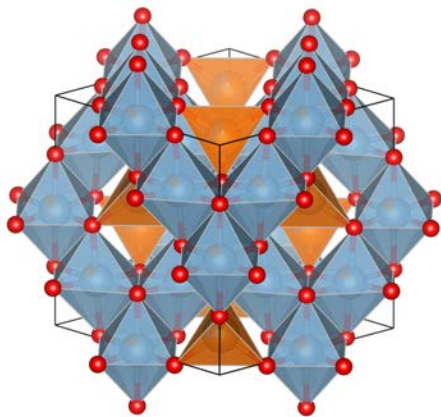


Al-Phase at High Pressure

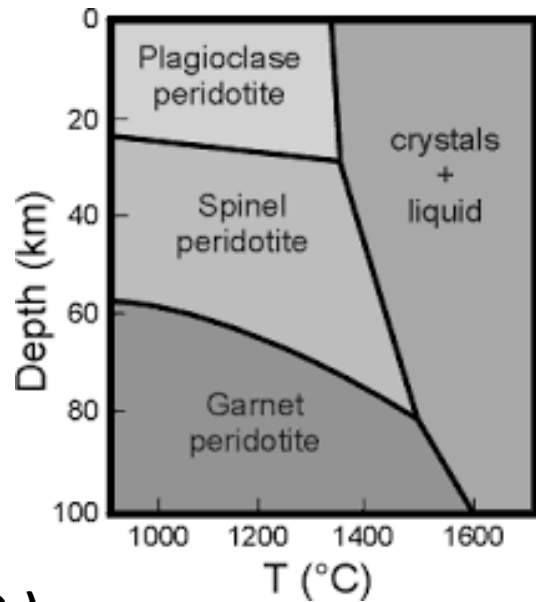
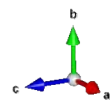
Plagioclase ($\text{Ca}[\text{Al}_2\text{Si}_2\text{O}_8]\text{-Na}[\text{AlSi}_3\text{O}_8]$)



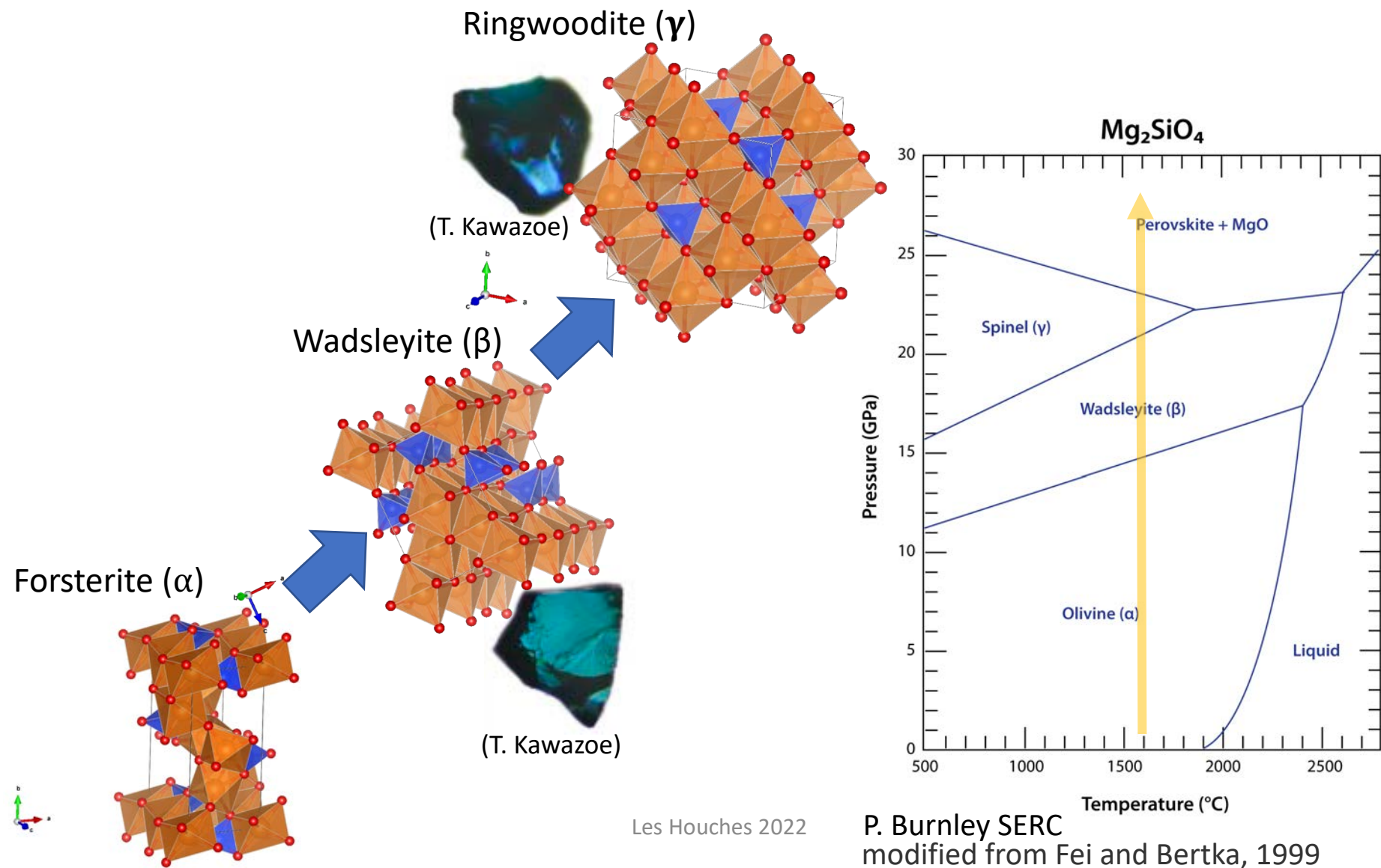
Spinel MgAl_2O_4



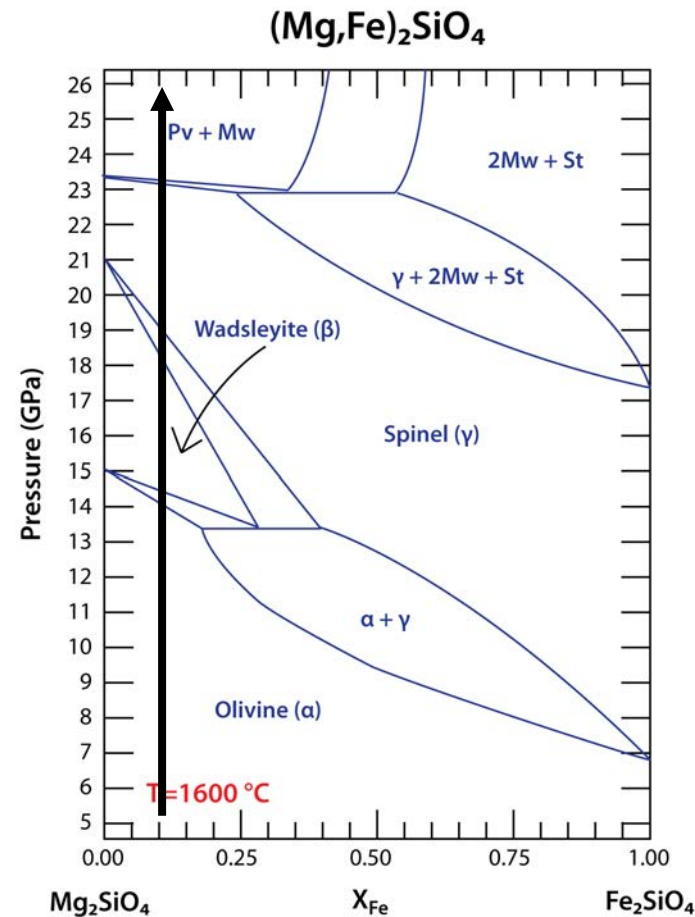
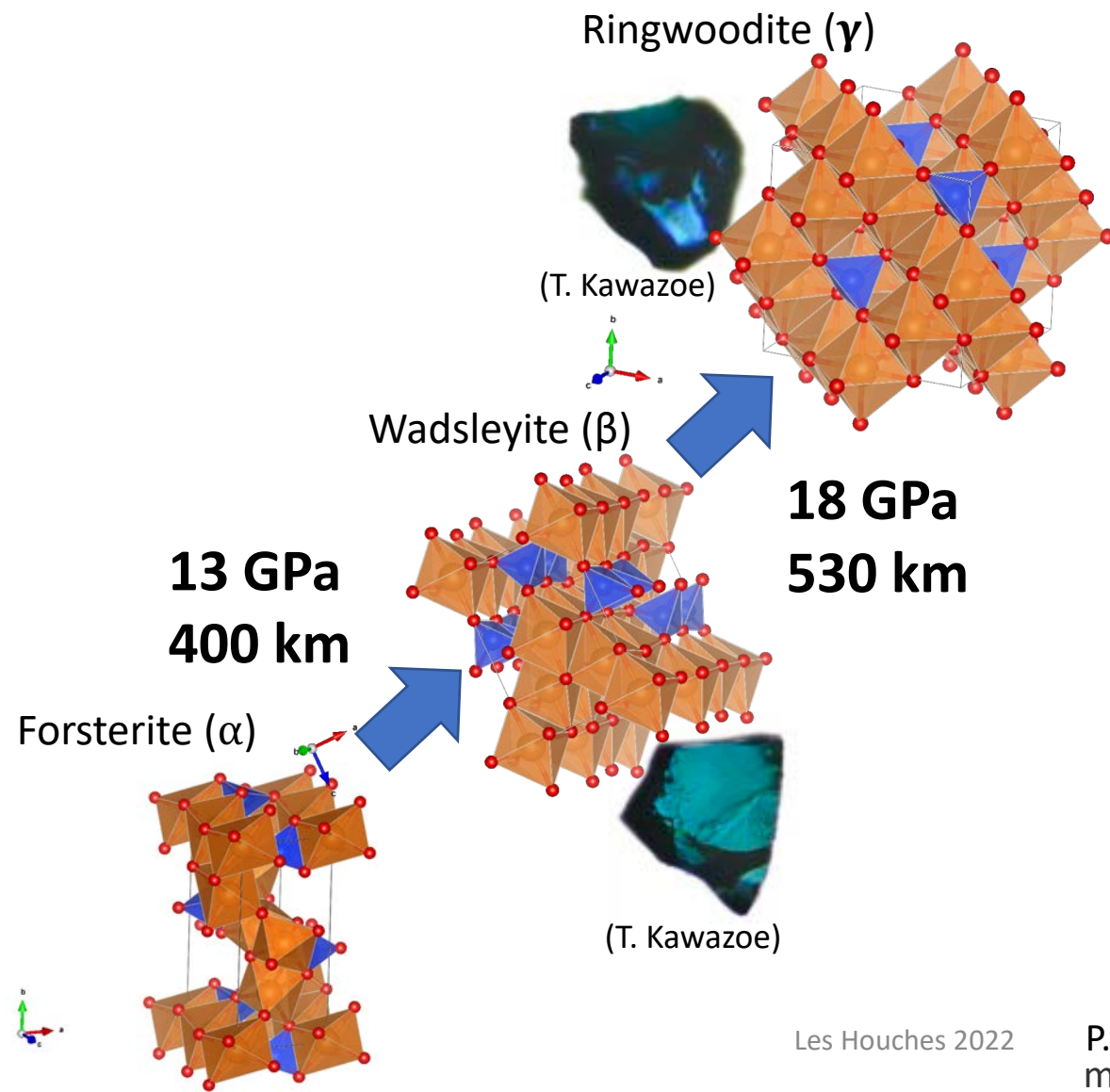
Garnet $\text{Mg}_3\text{Al}_2(\text{SiO}_4)_3$



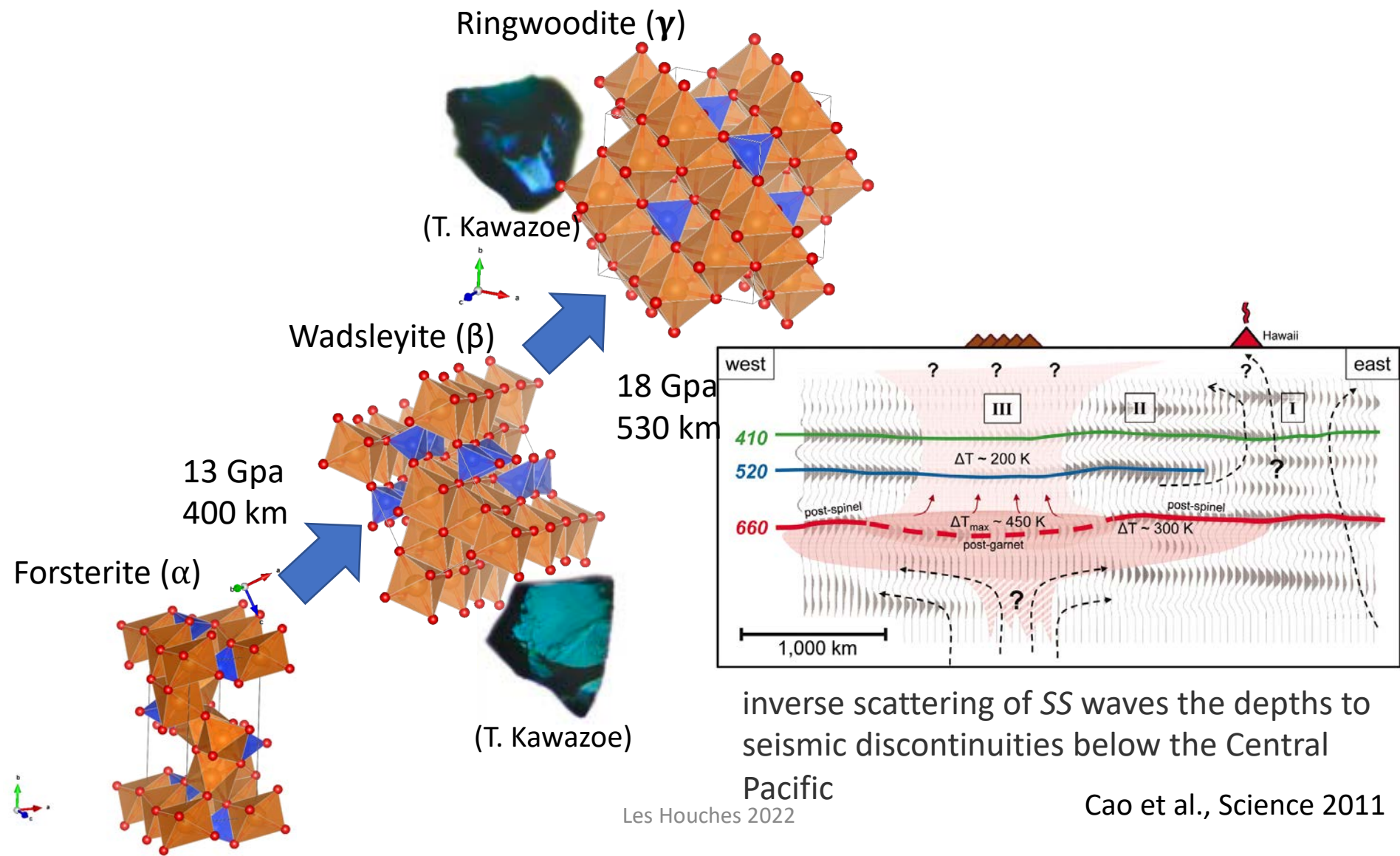
Phase Transitions of Olivine



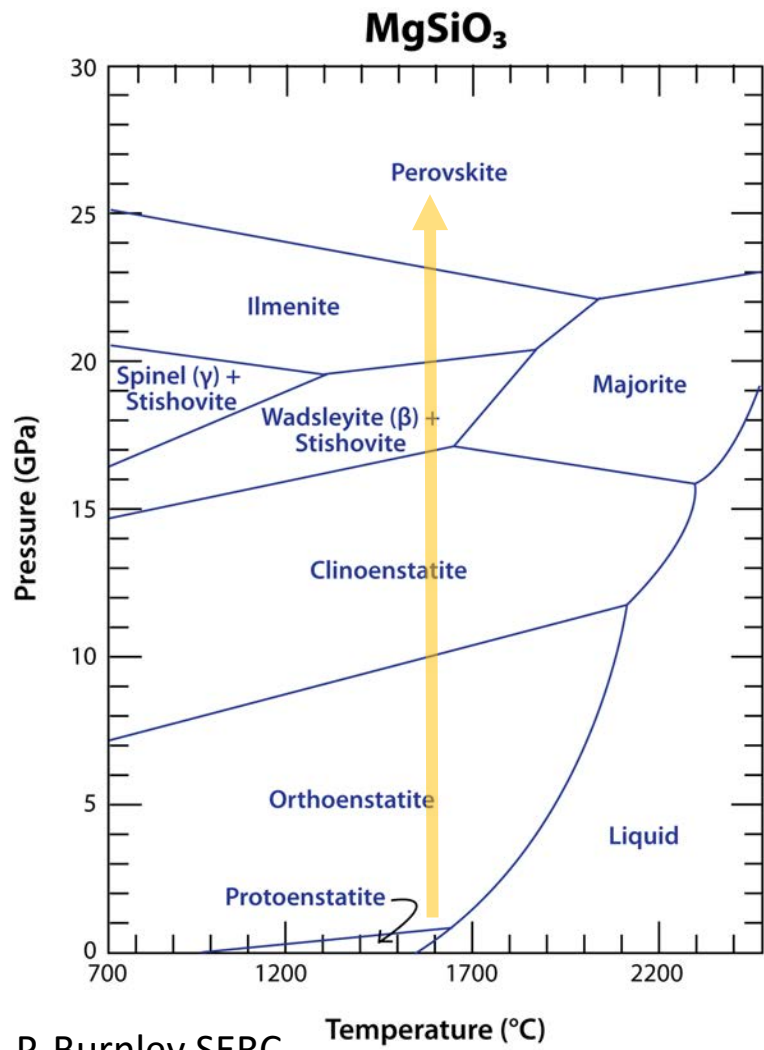
Phase Transitions of Olivine



Phase Transitions of Olivine



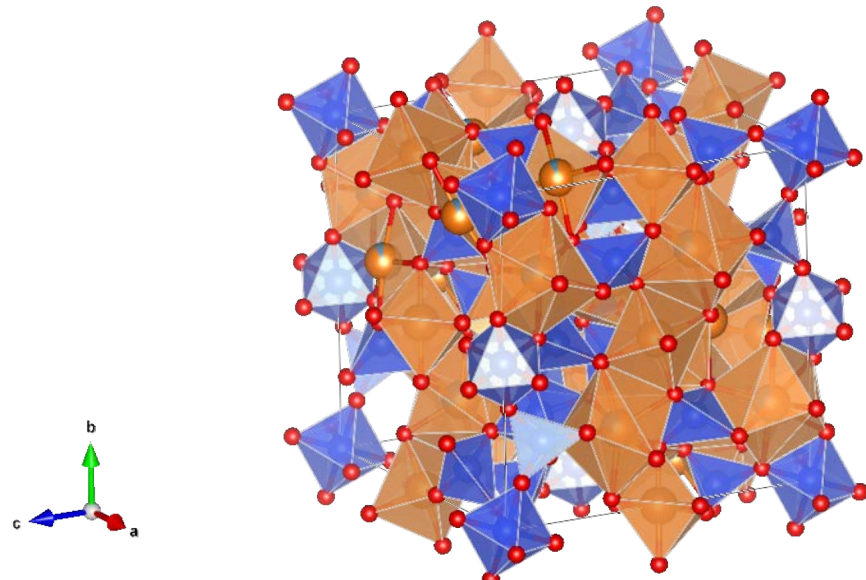
Phase Transitions of Pyroxenes



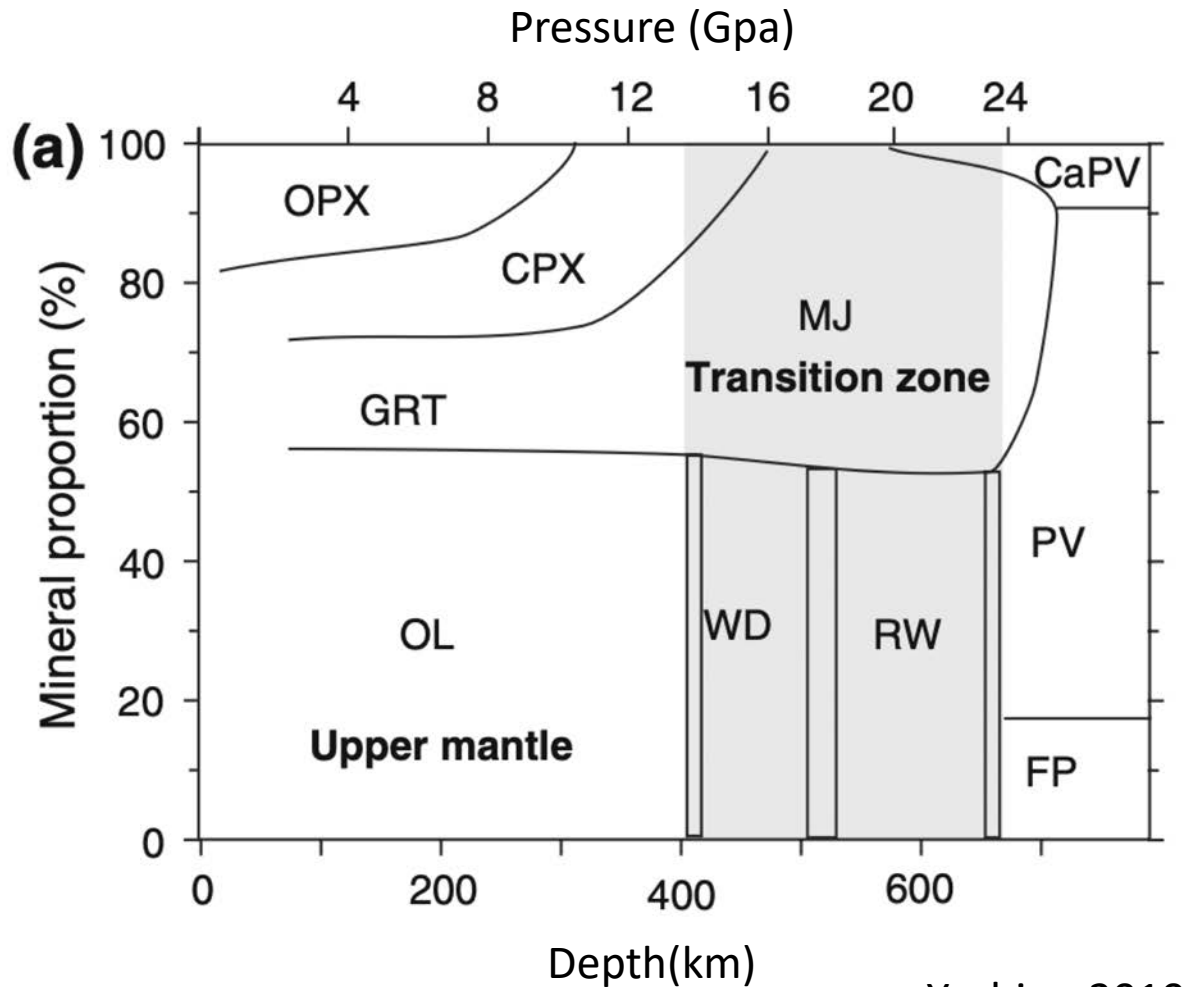
modified from Fei and Bertka, 1999

Majorite

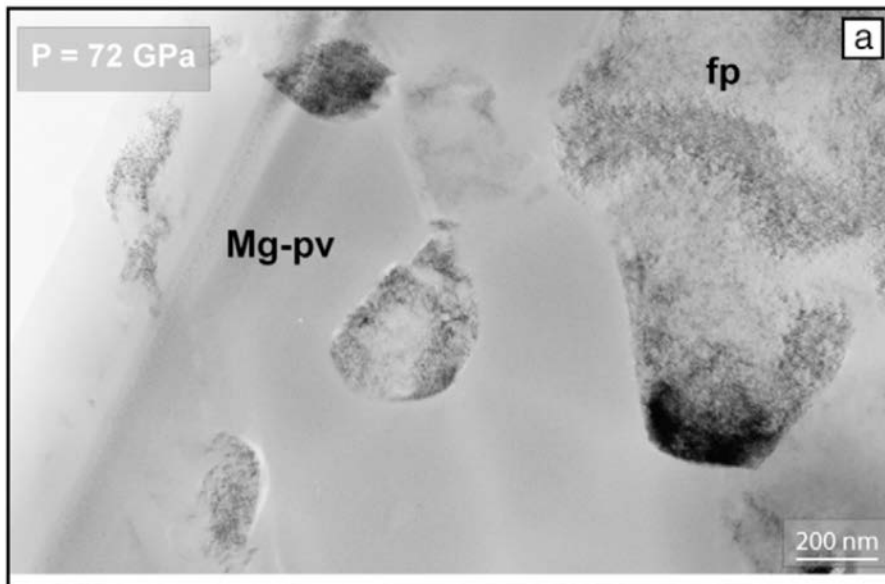
Mg₃(MgSi)(SiO₄)₃ Incorporates Fe,Ca, Al ...



Mineral Proportion in the Mantle

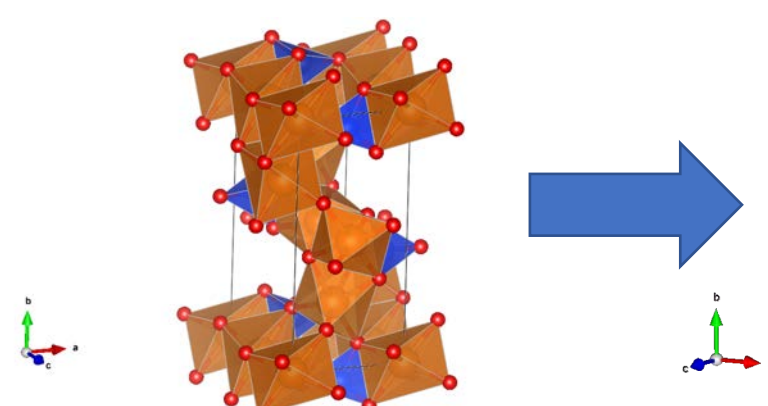


Transition to the Lower Mantle

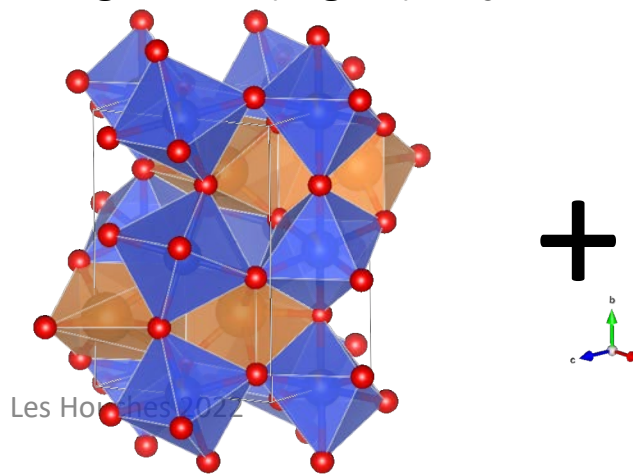


Olivine tranformed
at 72 Gpa - HT
Auzende et al. 2008

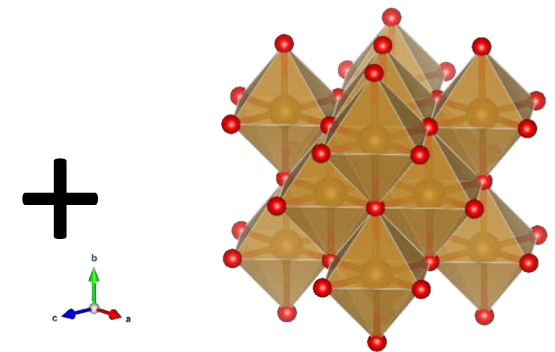
Forsterite (α)



Bridgmanite $(\text{Mg}, \text{Fe})\text{SiO}_3$

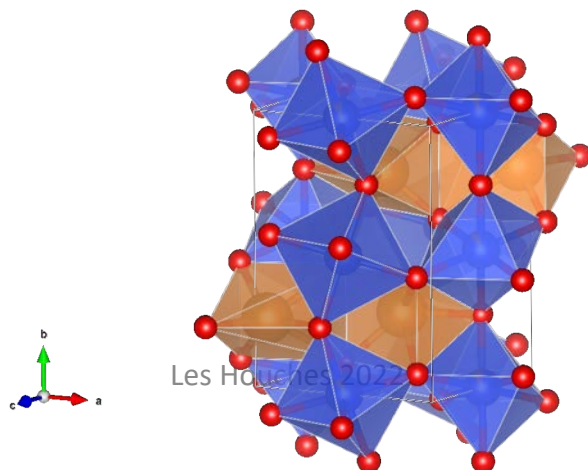


Ferropericlase $(\text{Mg}, \text{Fe})\text{O}$

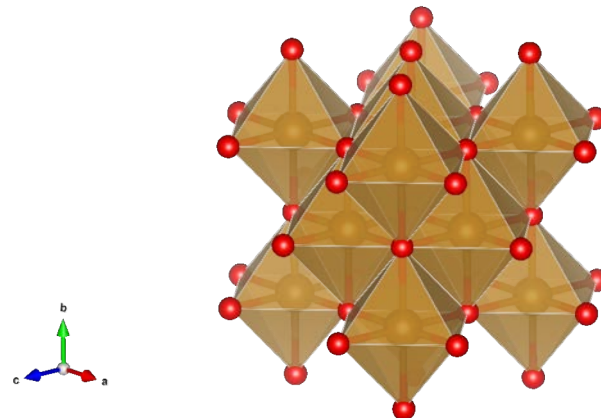


Lower Mantle Mineralogy

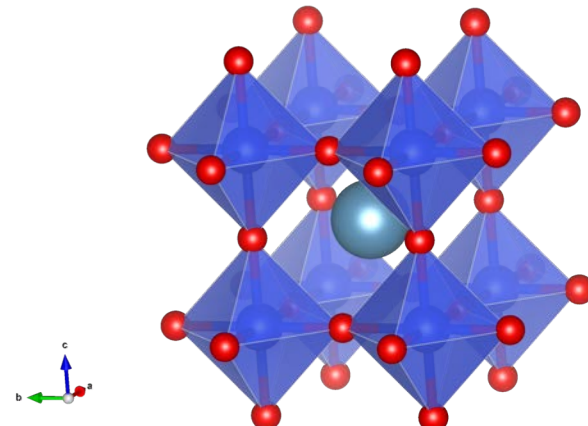
Bridgmanite $(\text{Mg},\text{Fe})\text{SiO}_3$



Ferropericlase $(\text{Mg},\text{Fe})\text{O}$



Davemaoite CaSiO_3



Les Houches 2022

Lower Mantle Mineralogy

Bridgmanite

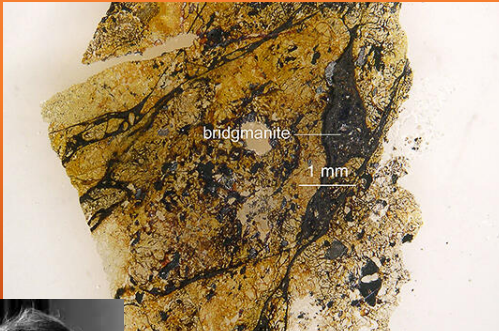
MINERALOGY

Science 2014

Discovery of bridgmanite, the most abundant mineral in Earth, in a shocked meteorite

Oliver Tschäuner,^{1*} Chi Ma,² John R. Beckett,² Clemens Prescher,³ Vitali B. Prakapenka,³ George R. Rossman²

Meteorites exposed to high pressures and temperatures during impact-induced shock often contain minerals whose occurrence and stability normally confine them to the deeper portions of Earth's mantle. One exception has been MgSiO_3 in the perovskite structure, which is the most abundant solid phase in Earth. Here we report the discovery of this important phase as a mineral in the Tenham L6 chondrite and approved by the International Mineralogical Association (specimen IMA 2014-017). MgSiO_3 -perovskite is now called bridgmanite. The associated phase assemblage constrains peak shock conditions to ~ 24 gigapascals and 2300 kelvin. The discovery concludes a half century of efforts to find, identify, and characterize a natural specimen of this important mineral.



Hiroseite

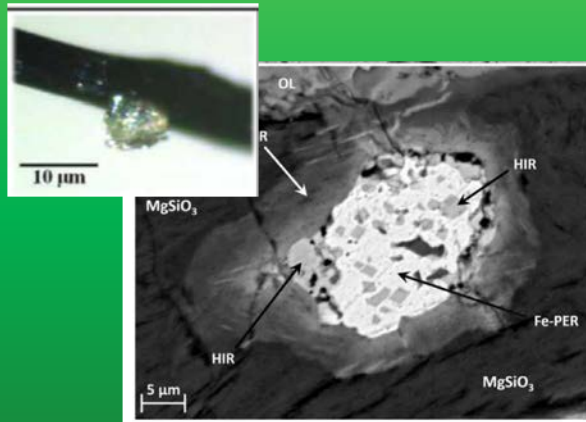
SCIENCE /
GEOLOGY

Science Advances, 2020

Evidence for the charge disproportionation of iron in extraterrestrial bridgmanite

Luca Bindi^{1*}, Sang-Heon Shim², Thomas G. Sharp², Xiande Xie³

Bridgmanite, MgSiO_3 with perovskite structure, is considered the most abundant mineral on Earth. On the lower mantle, it contains Fe and Al that strongly influence its behavior. Experimentalists have debated whether iron may exist in a mixed valence state, codexistence of Fe^{2+} and Fe^{3+} in bridgmanite, through charge disproportionation. Here, we report the discovery of Fe-rich aluminous bridgmanite coexisting with metallic iron in a shock vein of the Suizhou meteorite. This is the first direct evidence in nature of the Fe disproportionation reaction, which so far has only been observed in some high-pressure experiments. Furthermore, our discovery supports the idea that the disproportionation reaction would have played a key role in redox processes and the evolution of Earth.



Davemaoite

RESEARCH

MINERALOGY

Science, 2021

Discovery of dave Maoite, CaSiO_3 -perovskite, as a mineral from the lower mantle

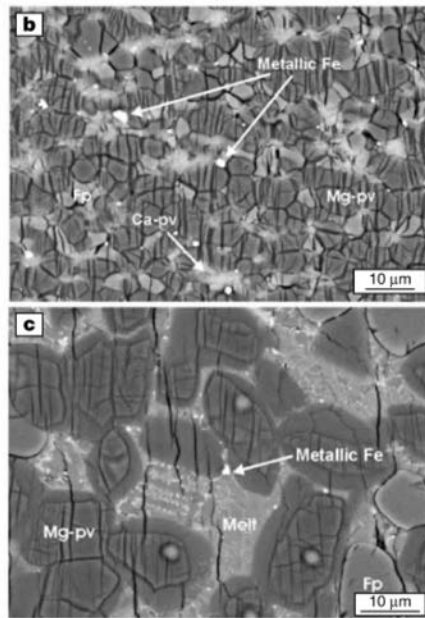
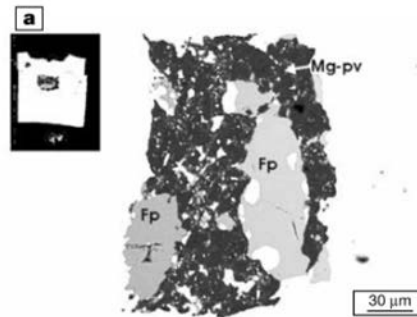
Oliver Tschäuner¹, Shichun Huang¹, Shuying Yang², Munir Humayun², Wenjun Liu³, Stephanie N. Gilbert Corder⁴, Hans A. Bechtel⁴, Jon Tischler⁵, George R. Rossman⁶

Calcium silicate perovskite, CaSiO_3 , is arguably the most geochemically important phase in the lower mantle, because it concentrates elements that are incompatible in the upper mantle, including the heat-generating elements thorium and uranium, which have half-lives longer than the geologic history of Earth. We report CaSiO_3 -perovskite as an approved mineral (IMA2020-012a) with the name dave Maoite. The natural specimen of dave Maoite proves the existence of compositional heterogeneity within the lower mantle. Our observations indicate that dave Maoite also hosts potassium in addition to uranium and thorium in its structure. Hence, the regional and global abundances of dave Maoite influence the heat budget of the deep mantle, where the mineral is thermodynamically stable.



Bridgmanite Fe Disproportionation

Al-pyroxene + Fe
Multi-anvil exp.



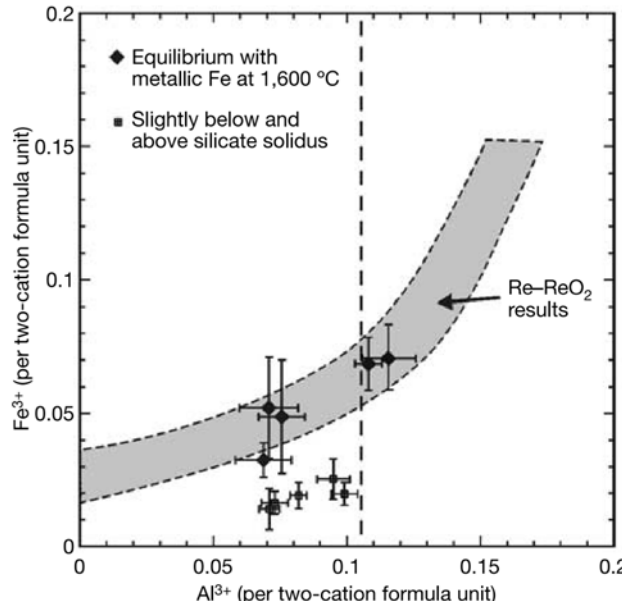
Al-Bearing Bridgmanite : $(\text{Mg}, \text{Fe})(\text{Si}, \text{Al})\text{O}_3$



Favorable up to 100 GPa

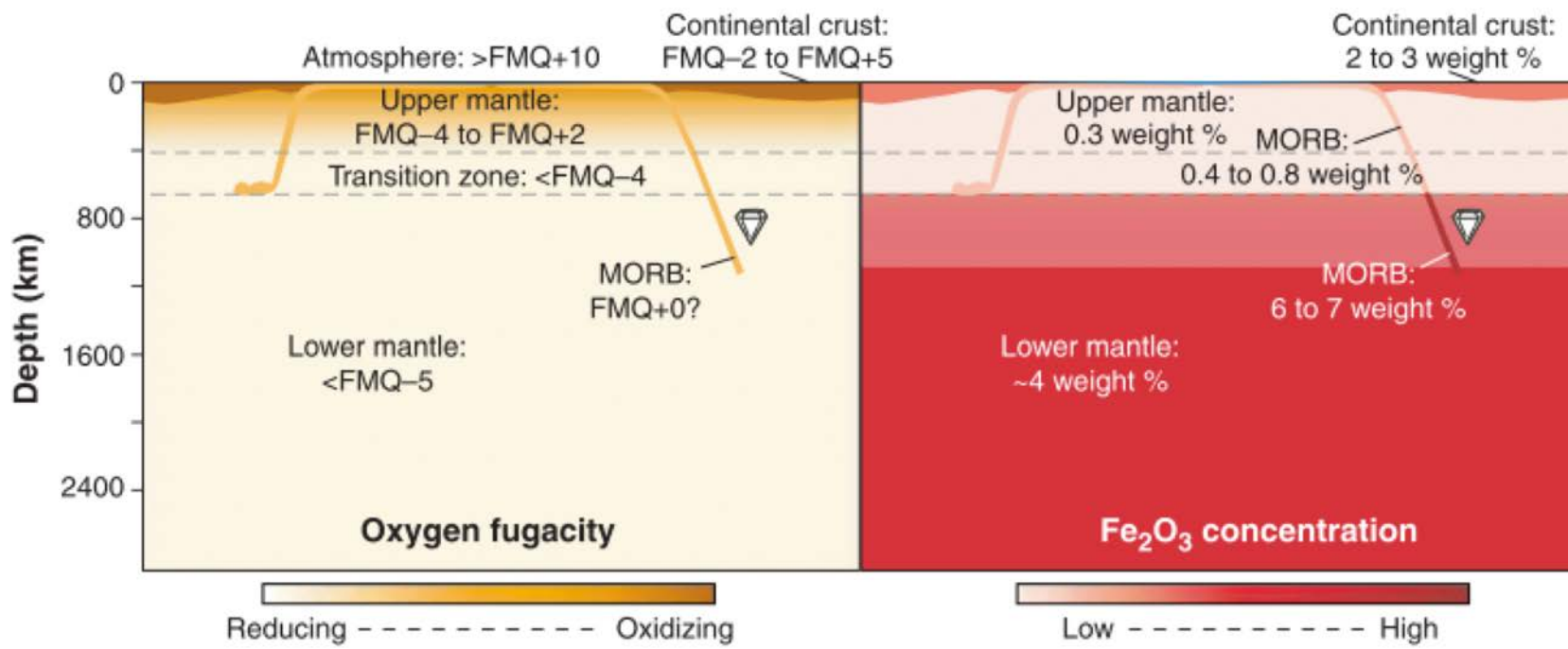
Fe³⁺ content not sensitive to the oxygen fugacity but to Al content

The Lower mantle is saturated in metal Fe



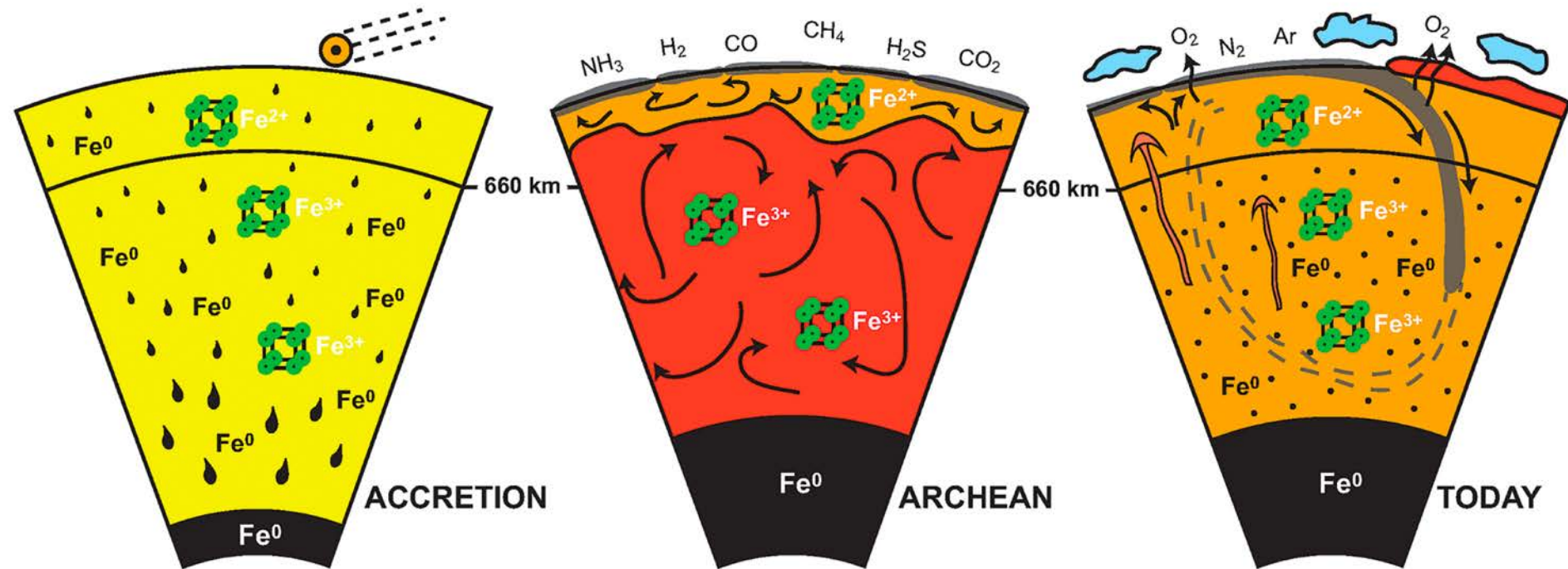
Bridgmanite Fe Disproportionation

Mantle Paradigm :

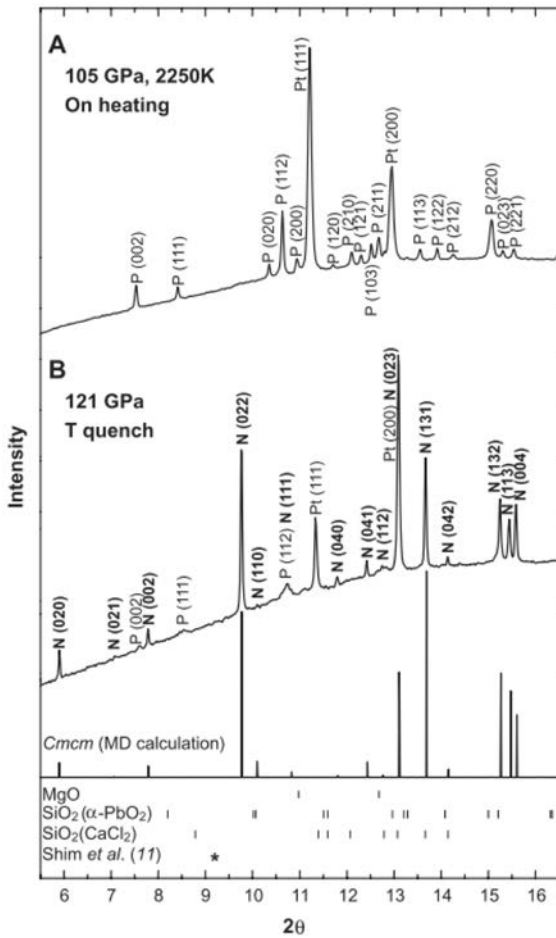


McCammon, Science 2005

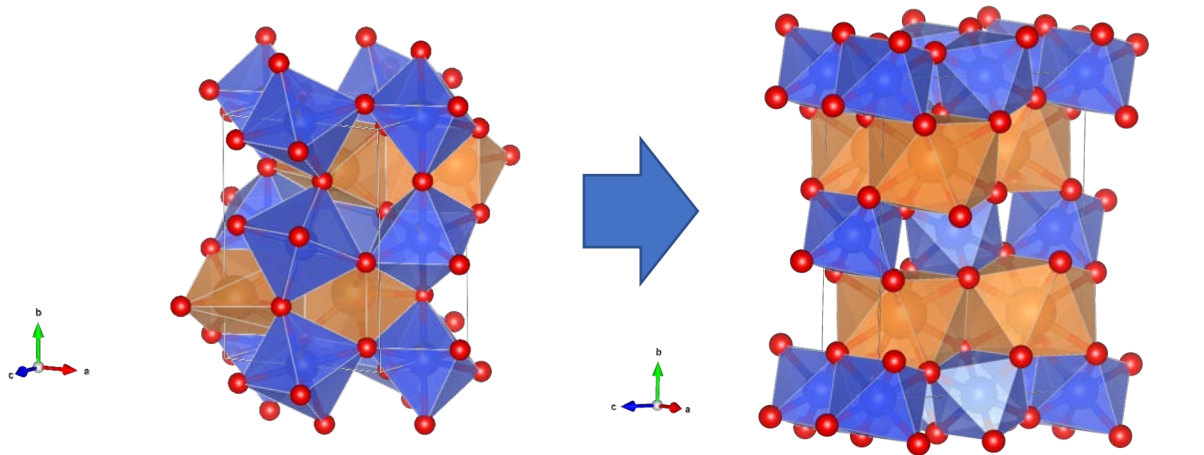
Bridgmanite Fe Disproportionation



Core Mantle Boundary



Murakami, Science 2004



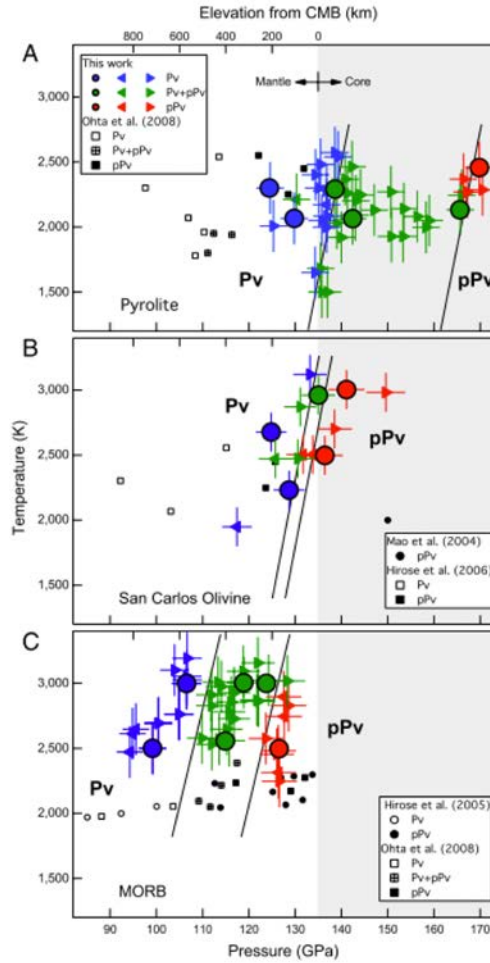
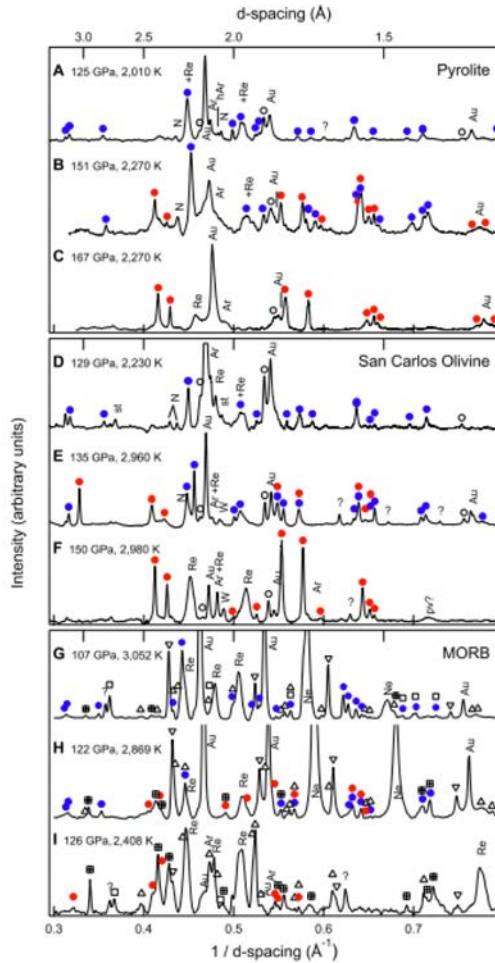
Bridgmanite (Mg,Fe)SiO₃

Post-Perovskite (Mg,Fe)SiO₃

Preferred orientation in subducting slab => seismic anisotropy

➤ Is D'' a Mineralogical Transition ?

Is D'' a Mineralogical Transition ?



Grocholski et al., 2012

Les Houches 2022



Mineral Evolution

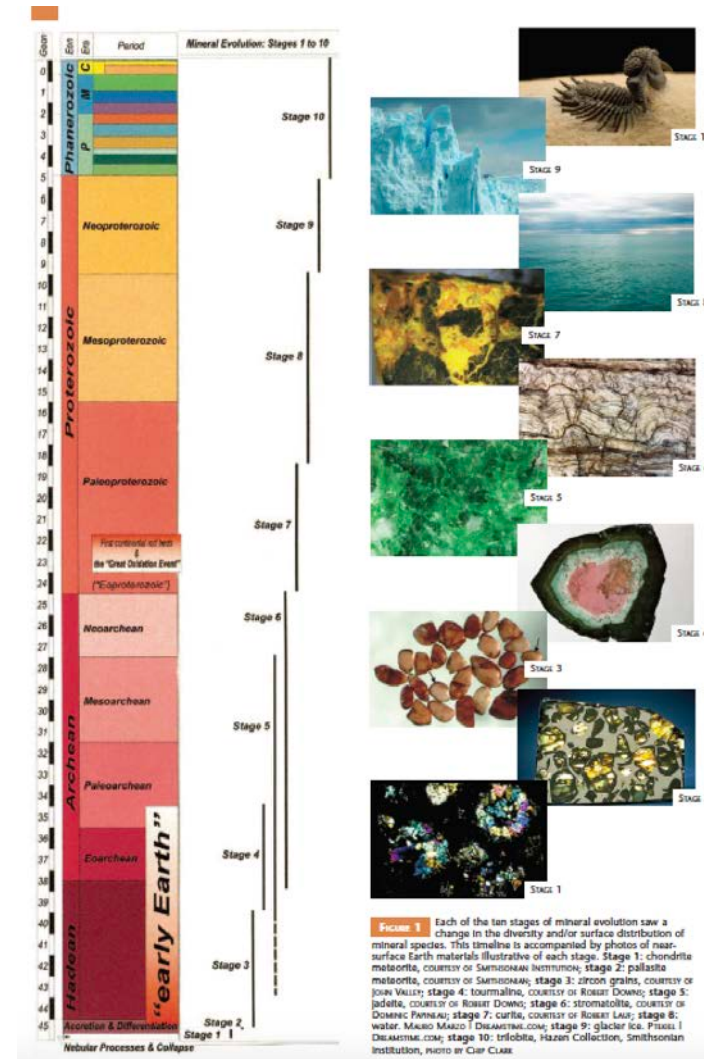
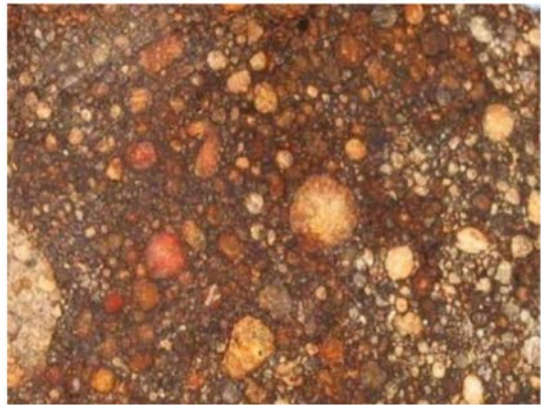


FIGURE 1 Each of the ten stages of mineral evolution saw a change in the diversity and/or surface distribution of mineral species. This figure is accompanied by photographs of near-surface Earth materials illustrating each stage. Stage 1: chondrite meteorite, courtesy of SMITHSONIAN INSTITUTION; stage 2: pallaseite meteorite, courtesy of SMITHSONIAN; stage 3: zircon grains, courtesy of ROBIN DOWD; stage 4: tourmaline, courtesy of ROBIN DOWD; stage 5: jadesite, courtesy of ROBIN DOWD; stage 6: stromatolite, courtesy of DOMINIEN PANNIUS; stage 7: corita, courtesy of ROBIN DOWD; stage 8: water ice, courtesy of ROBIN DOWD; stage 9: glacier, courtesy of DREAMTIME.COM; stage 10: trilobite, Hazen Collection, Smithsonian Institution, photo by CAP CLARK.

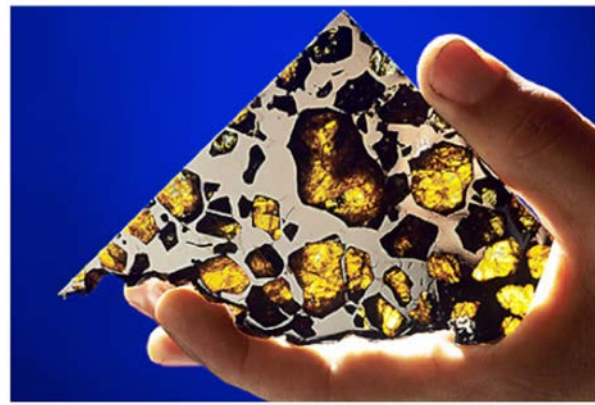


Hazen and Ferry (2010)

Mineral Evolution



**Stage 1 : stellar nebula
prior to planetary accretion**
Unaltered chondrites : 60
species



**Stage 2 : planetisimals
accretion and differentiation**
Lunar and meteorites : 250
species



Stage 3 : Earth's Differentiation
420 species (hydrous phases at
the poles)

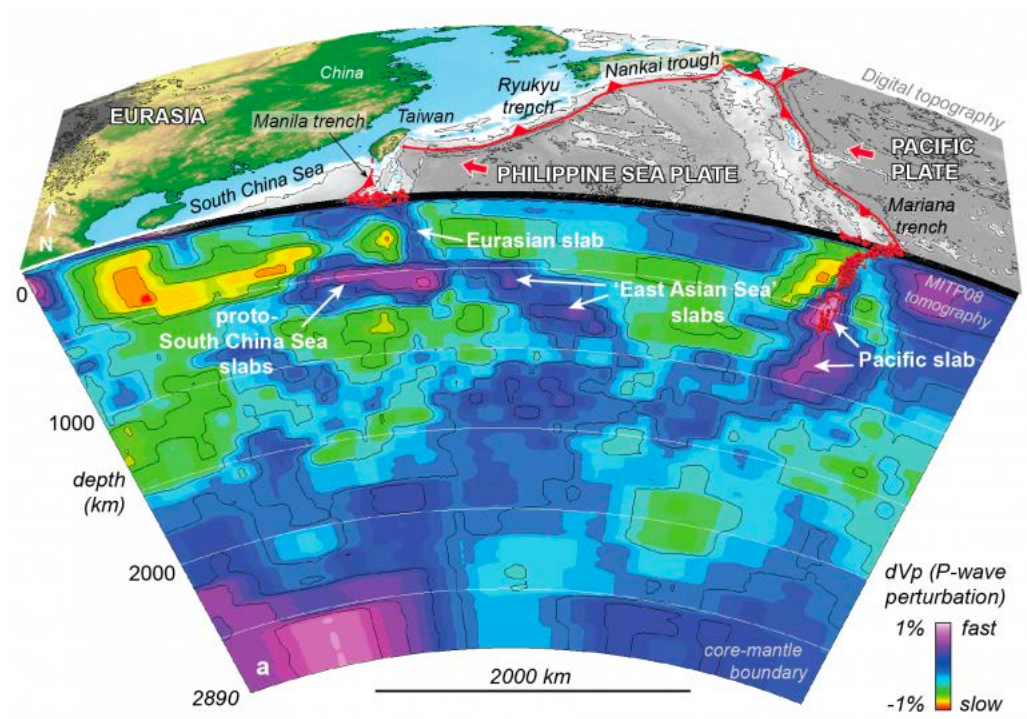


Deep Earth's mineralogy
- expends as pressure increases,
temperature decreases
- Differentiation = extract iron etc..

Hazen 2013

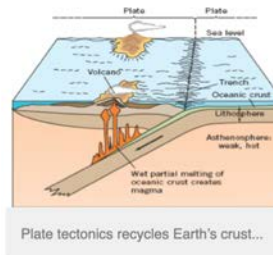
Homogenous Mantle?

Homogenous Mantle?



Li et al., G³, 2008

Mineral Evolution



and leads to new modes of volcanism...



...with associated production of massive sulfide ore deposits.



Copper sulfides covellite and djurleite

**Stage 4 : continents
granite and pegmatite**



Tectonic processes lead to the generation and exposure of high-pressure minerals, including:



Staurolite. Photo by Rob Lavinsky



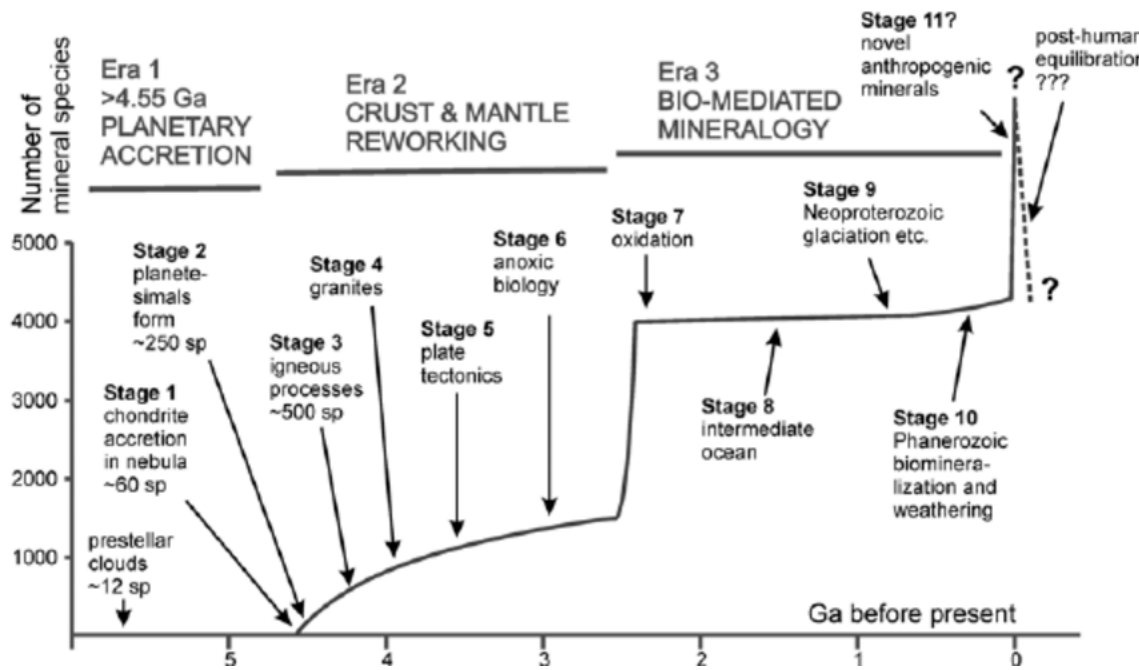
Jadeite. Photo by Rob Lavinsky



Kyanite.
Photo by
Rob
Lavinsky

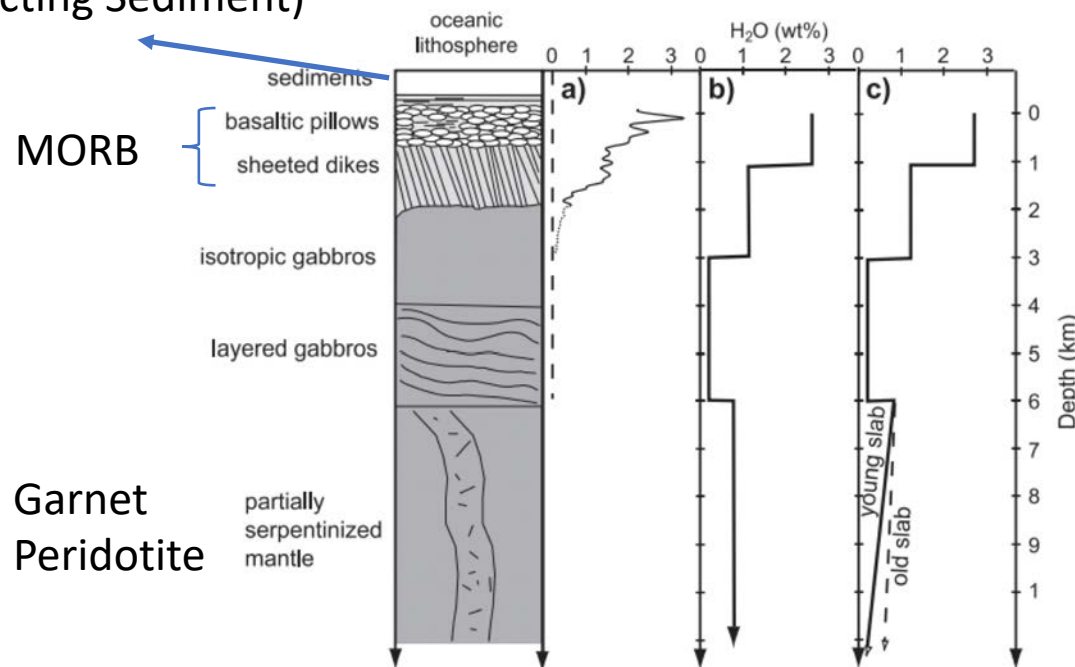
**Stage 5 : global scale plate tectonics
+ 1500 species**

Mineral Evolution



Slab Composition

GLOSS
GLObal Subducting Sediment)



Rüpke, EPSL, 2004

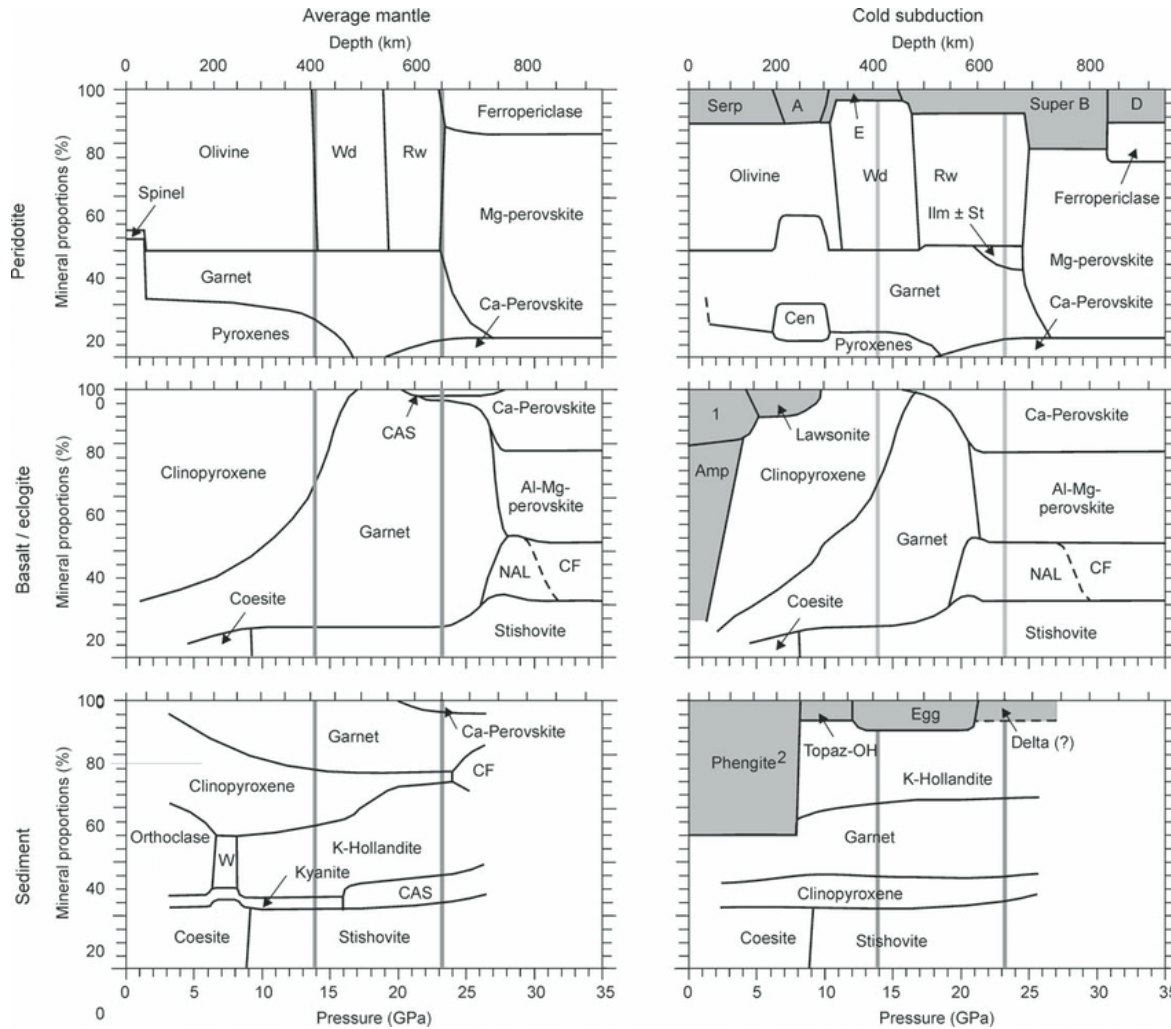
Slab Chemical Composition

Sample	Pyrolite (1)	Pyrolite (2)	Piclogite (3)	C1 (4)	Lherzolite (5)	Harzburgite (5)	Dunite (5)
SiO ₂	45.1	45.0	47.0	22.01	39.53	40.39	38.37
TiO ₂	0.2	0.20	0.4	0.07	0.32		0.11
Al ₂ O ₃	4.3	4.45	8.6	1.55	2.62	0.85	1.06
Cr ₂ O ₃	0.4	0.38	0.2	0.37	0.20	0.40	0.24
FeO	8.0	8.05	10.8	22.84	11.15	9.65	11.54
MnO	0.1	0.135	0.1	0.24	0.20	0.14	0.13
MgO	38.1	37.80	24.0	15.34	32.95	36.71	36.28
NiO	0.2	0.25	0.1	1.32	0.25	0.25	0.25
CaO	3.1	3.55	8.0	1.26	1.95	0.93	0.60
Na ₂ O	0.4	0.36	1.0	0.65	0.30	0.04	0.05
K ₂ O	0.03	0.029	0.1	0.06	0.03	0.01	0.01
P ₂ O ₅	0.02	0.021		0.20	0.02		0.03
H ₂ O		0.090		17.51 [†]	9.49	9.76	10.33
CO ₂		0.044		11.36			
Total	99.55	100.37	100.3	100.0	99.01	99.13	99.00
Sample	MORB (6)	Altered MORB (7)	Fe-gabbro (8)	Gabbro (5)	Troctolite (5)	Volcanoclastic (9)	Red clay (9)
SiO ₂	50.45	45.80	46.78	44.28	41.09	55.97	52.60
TiO ₂	1.62	1.18	4.47	0.28	0.08	1.03	0.67
Al ₂ O ₃	15.26	15.53	11.30	16.00	25.89	12.51	14.01
FeO	10.43	9.01	17.02	4.05	4.73	7.36	7.81
MnO	0.17	0.17	0.26	0.10	0.11	0.26	1.68
MgO	7.58	6.66	6.72	10.05	10.14	5.39	3.05
CaO	11.30	12.88	9.18	18.28	9.83	5.25	3.14
Na ₂ O	2.68	2.07	3.85	0.60	1.62	3.21	2.79
K ₂ O	0.11	0.56	0.10	0.05	0.06	1.67	2.84
P ₂ O ₅	0.15	0.11	0.32	0.05	0.05	0.24	0.66
H ₂ O	0.25	2.68		5.71	5.86	6.25	10.04
CO ₂		2.95				0.73	0.39
Total	100.0	99.6	100.0	99.45	99.46	99.87	99.68
Sample	Silicic (9)	Terrigenous (9)	Shale (9)	Carbonate (9)	Ophicarbonate (10)	GLOSS (9)	Upper cont. crust (12) (11)
SiO ₂	71.56	59.26	62.0	32.79	28.51	58.57	66.0
TiO ₂	0.41	0.74	1.0	0.18	0.02	0.62	0.5
Al ₂ O ₃	8.07	15.53	15.9	3.99	0.43	11.91	15.2
FeO	3.99	5.88	6.5	2.40	1.27	5.21	4.5
MnO	0.38	0.17	0.1	0.25	0.04	0.32	0.11
MgO	1.69	2.46	2.2	1.43	25.61	2.48	2.2
CaO	1.08	2.78	1.3	30.41	13.41	5.95	4.2
Na ₂ O	2.39	2.78	1.2	1.58	0.33	2.43	3.9
K ₂ O	1.52	2.11	3.7	0.61	0.28	2.04	3.4
P ₂ O ₅	0.22	0.19	0.1	0.17	0.04	0.19	0.2
H ₂ O	8.49	8.22	6.0	2.82	18.27	7.29	
CO ₂	0.08			23.31	11.41	3.01	
Total	99.88	100.12	100.0	99.94	99.62	100.0	98.39

Litasov and Ohtani, 2007

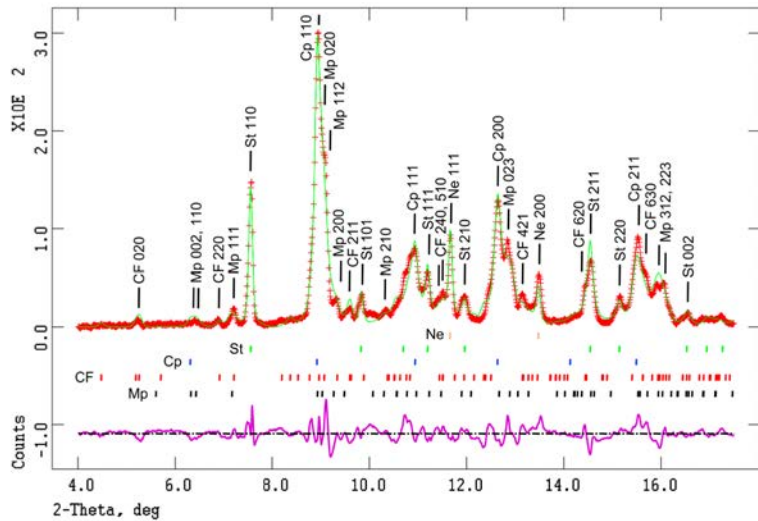
Slab Mineral Composition

- More SiO_2
- More Al_2O_3
- More CaO
- Lower MgO

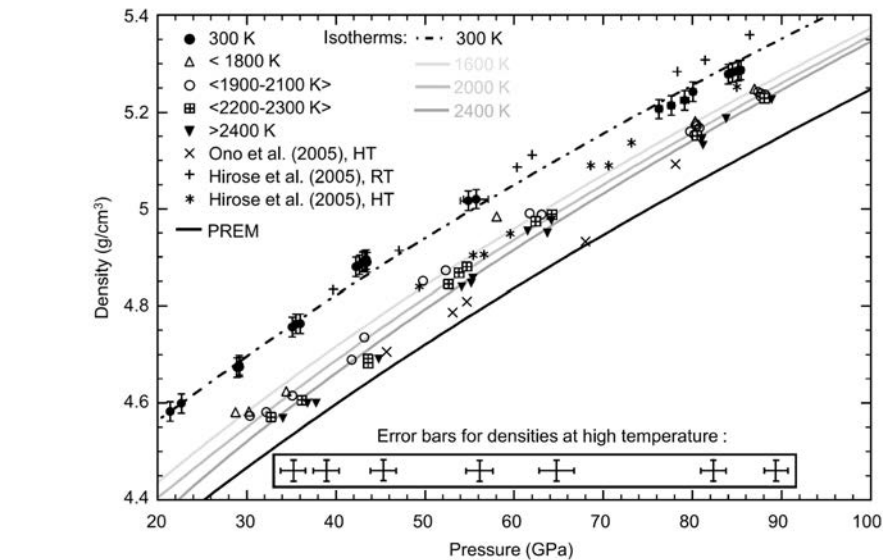
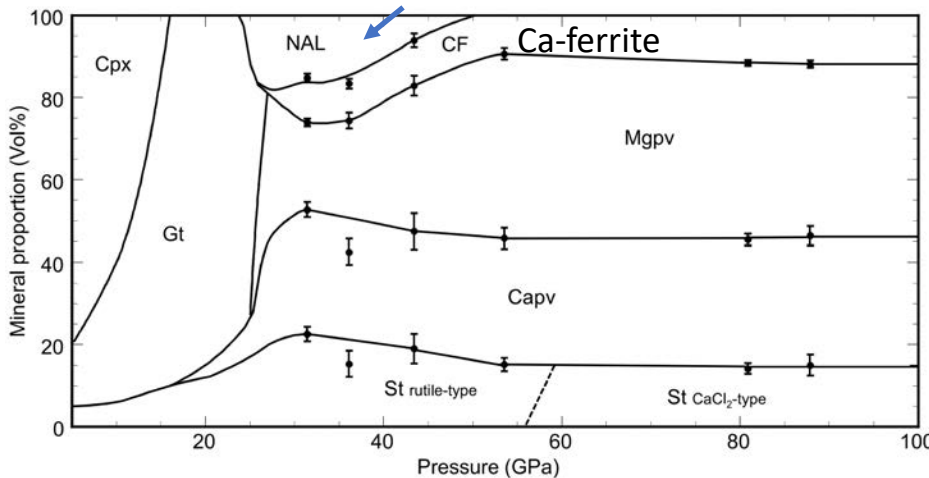


MORB at Mantle Conditions

MORB at 53 GPa and 2200 K :



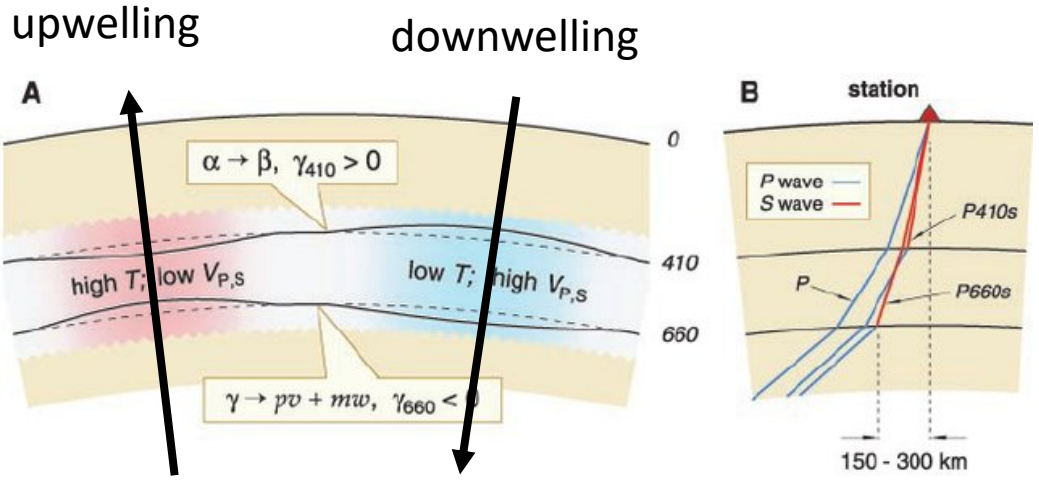
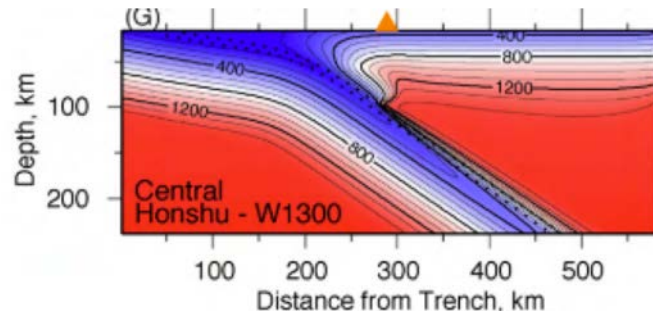
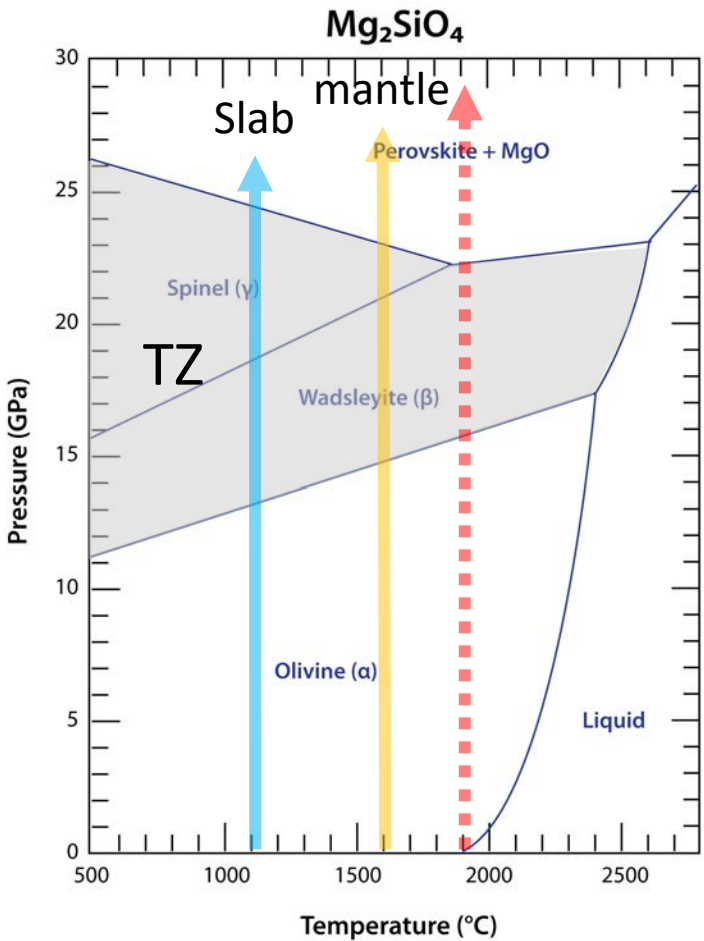
New Aluminium-rich Phase



2022

Ricolleau et al., 2010

Transition Zone Within Slab



Lebedev et al., Science 2002

Les Houches 2022

Slab Chemical Composition

Sample	Pyrolite (1)	Pyrolite (2)	Piclogite (3)	C1 (4)	Lherzolite (5)	Harzburgite (5)	Dunite (5)
SiO ₂	45.1	45.0	47.0	22.01	39.53	40.39	38.37
TiO ₂	0.2	0.20	0.4	0.07	0.32		0.11
Al ₂ O ₃	4.3	4.45	8.6	1.55	2.62	0.85	1.06
Cr ₂ O ₃	0.4	0.38	0.2	0.37	0.20	0.40	0.24
FeO	8.0	8.05	10.8	22.84	11.15	9.65	11.54
MnO	0.1	0.135	0.1	0.24	0.20	0.14	0.13
MgO	38.1	37.80	24.0	15.34	32.95	36.71	36.28
NiO	0.2	0.25	0.1	1.32	0.25	0.25	0.25
CaO	3.1	3.55	8.0	1.26	1.95	0.93	0.60
Na ₂ O	0.4	0.36	1.0	0.65	0.30	0.04	0.05
K ₂ O	0.03	0.029	0.1	0.06	0.03	0.01	0.01
P ₂ O ₅	0.02	0.021		0.20	0.02		0.03
H ₂ O		0.090		17.51 [†]	9.49	9.76	10.33
CO ₂		0.044		11.36			
Total	99.55	100.37	100.3	100.0	99.01	99.13	99.00
Sample	MORB (6)	Altered MORB (7)	Fe-gabbro (8)	Gabbro (5)	Troctolite (5)	Volcanoclastic (9)	Red clay (9)
SiO ₂	50.45	45.80	46.78	44.28	41.09	55.97	52.60
TiO ₂	1.62	1.18	4.47	0.28	0.08	1.03	0.67
Al ₂ O ₃	15.26	15.53	11.30	16.00	25.89	12.51	14.01
FeO	10.43	9.01	17.02	4.05	4.73	7.36	7.81
MnO	0.17	0.17	0.26	0.10	0.11	0.26	1.68
MgO	7.58	6.66	6.72	10.05	10.14	5.39	3.05
CaO	11.30	12.88	9.18	18.28	9.83	5.25	3.14
Na ₂ O	2.68	2.07	3.85	0.60	1.62	3.21	2.79
K ₂ O	0.11	0.56	0.10	0.05	0.06	1.67	2.84
P ₂ O ₅	0.15	0.11	0.32	0.05	0.05	0.24	0.66
H ₂ O	0.25	2.68		5.71	5.86	6.25	10.04
CO ₂		2.95				0.73	0.39
Total	100.0	99.6	100.0	99.45	99.46	99.87	99.68
Sample	Silicic (9)	Terrigenous (9)	Shale (9)	Carbonate (9)	Ophicarbonate (10)	GLOSS (9)	Upper cont. crust (12) (11)
SiO ₂	71.56	59.26	62.0	32.79	28.51	58.57	66.0
TiO ₂	0.41	0.74	1.0	0.18	0.02	0.62	0.5
Al ₂ O ₃	8.07	15.53	15.9	3.99	0.43	11.91	15.2
FeO	3.99	5.88	6.5	2.40	1.27	5.21	4.5
MnO	0.38	0.17	0.1	0.25	0.04	0.32	0.11
MgO	1.69	2.46	2.2	1.43	25.61	2.48	2.2
CaO	1.08	2.78	1.3	30.41	13.41	5.95	4.2
Na ₂ O	2.39	2.78	1.2	1.58	0.33	2.43	3.9
K ₂ O	1.52	2.11	3.7	0.61	0.28	2.04	3.2
P ₂ O ₅	0.22	0.19	0.1	0.17	0.04	0.19	3.4
H ₂ O	8.49	8.22	6.0	2.82	18.27	7.29	1.9
CO ₂	0.08			23.31	11.41	3.01	0.2
Total	99.88	100.12	100.0	99.94	99.62	100.0	98.39

Litasov and Ohtani, 2007

Water Transport in the Mantle



Newsroom Media & Communications Office

Newsroom Photos Videos Fact Sheets Lab History News Categories

Contact: [Karen McNulty Walsh](#), (631) 344-8350, or [Peter Genzer](#), (631) 344-3174

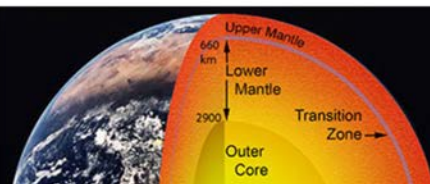
share:

The following news release on a paper published today in the journal *Science* was issued by Northwestern University. The research was conducted, in part, at the National Synchrotron Light Source at the U.S. Department of Energy's Brookhaven National Laboratory.

New Evidence for Oceans of Water Deep in the Earth

Water bound in mantle rock alters our view of the Earth's composition

June 13, 2014



[Home](#) > [World News](#) > [Scientists Discover Massive "Ocean" Near Earth's Core](#)

Scientists Discover Massive "Ocean" Near Earth's Core

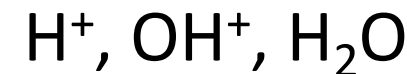
The study confirmed something that it was only a theory, namely that ocean water accompanies subducting slabs and thus enters the transition zone.

[World News](#) | Edited by Anjali Thakur | Updated: October 02, 2022 7:51 am IST

TRENDING

Watch: Epic No-Ball Drama On Last Delivery Of Bangladesh vs Zimbabwe Match

"Want Uniform Civil Code But BJP Is Bluffing": Arvind Kejriwal In Gujarat



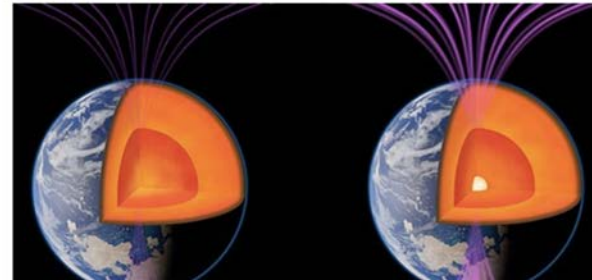
In hydrous phases
In nominally anhydrous phases as defect

Mis à jour le 29 septembre 2022, 11:02

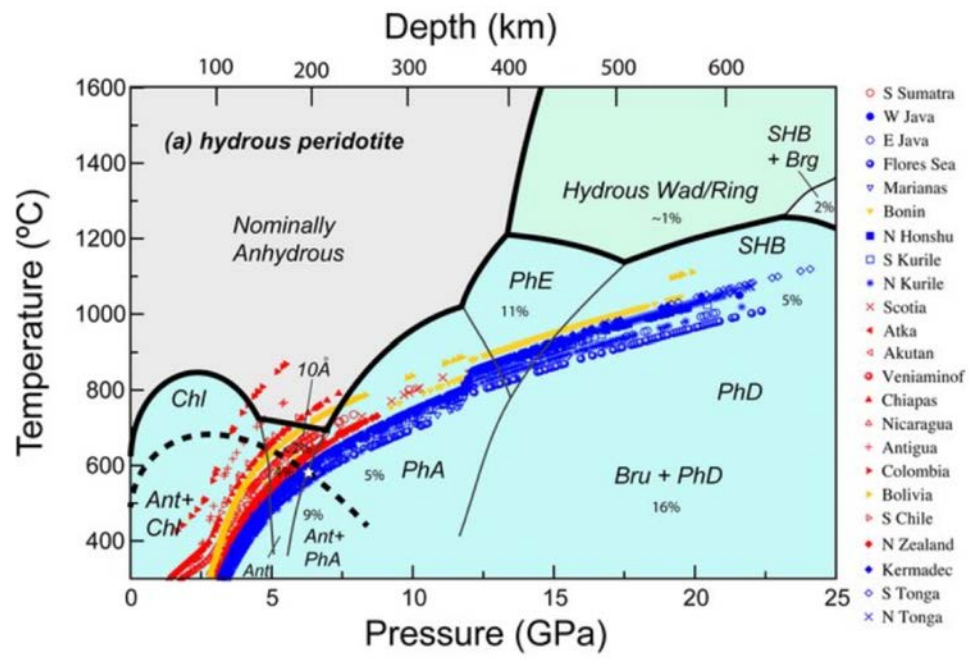
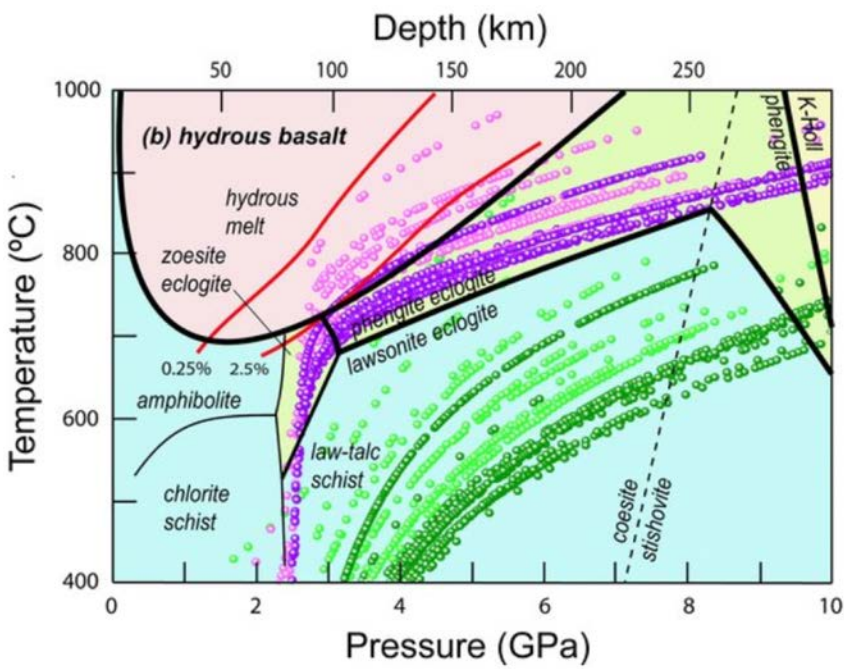
121 K lectures / 9 réactions

Des océans gigantesques dans les profondeurs de la Terre ?

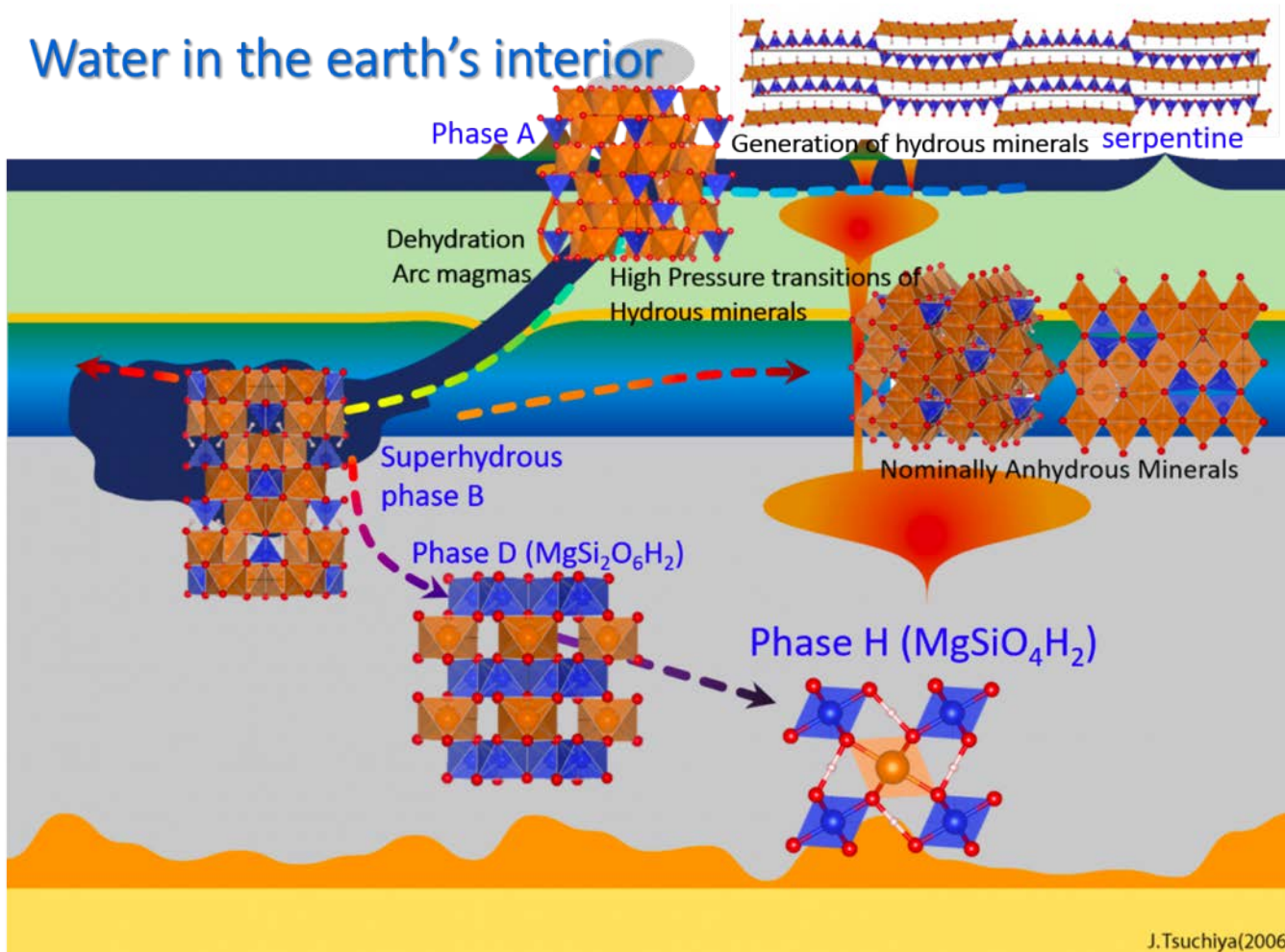
ACTUALITES DOSSIERS FAKE NEWS INDICATEURS AGENDA



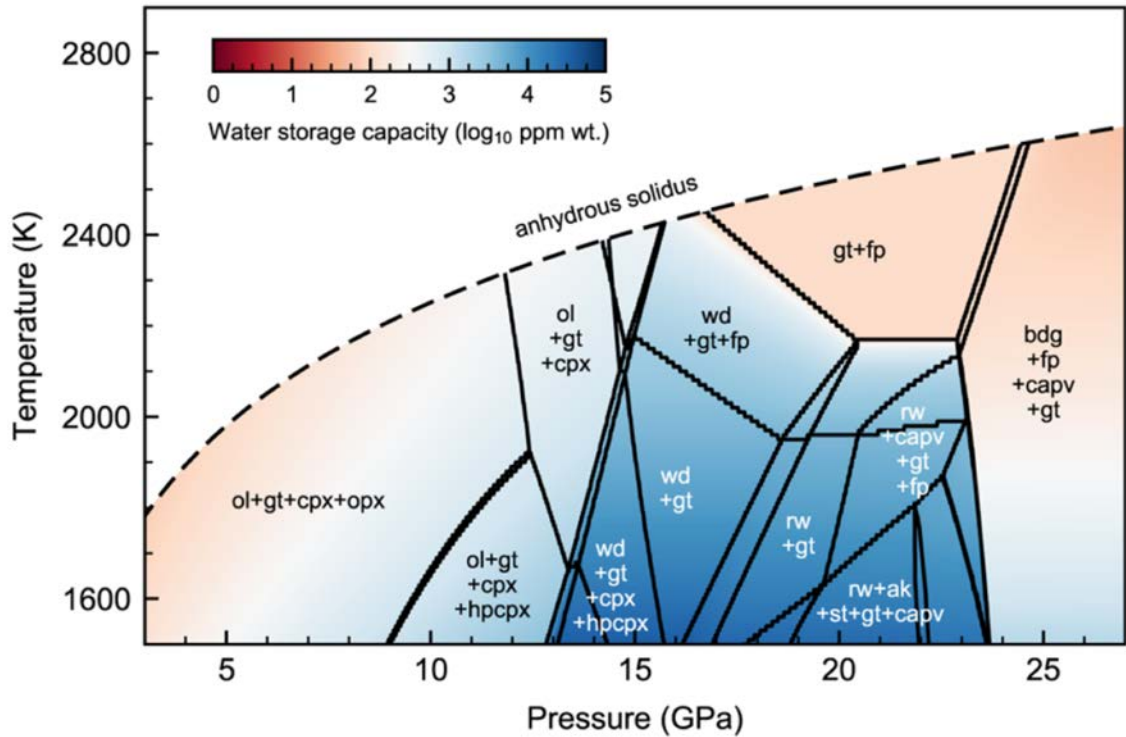
Water Transport in the Mantle



Dense Hydrous Magnesium Silicates



TZ : Nominally Anhydrous Phases

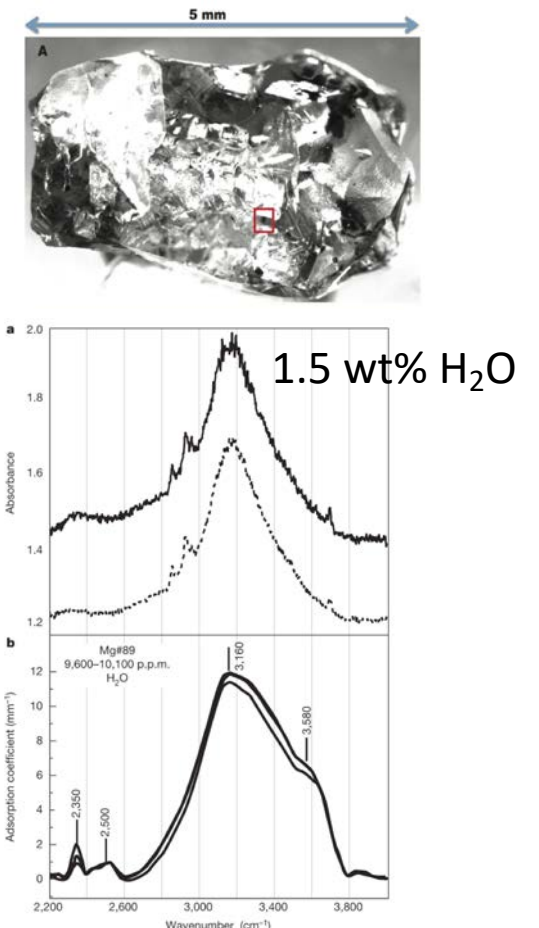


Dong et al., AGU Advances, 2012



Les Houches 2022

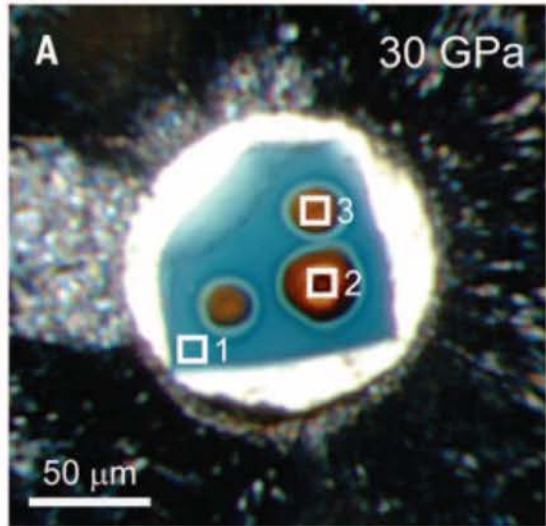
Ringwoodite Inclusions in natural diamonds



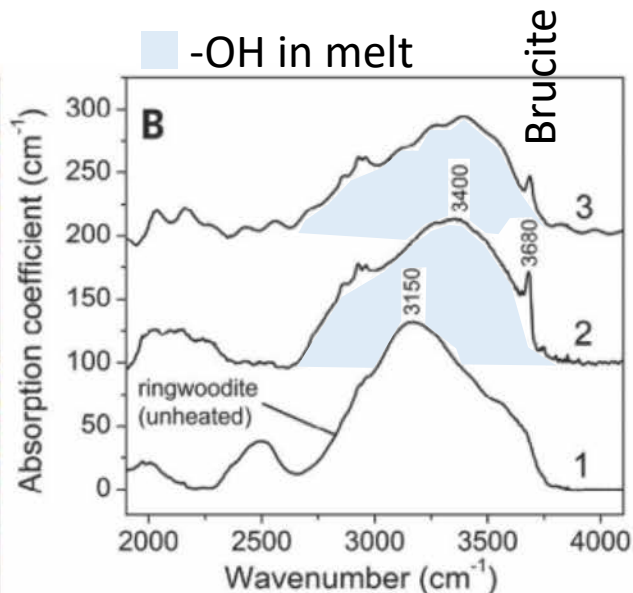
Pearson et al., Nature, 2014

Water Transport : TZ => LM

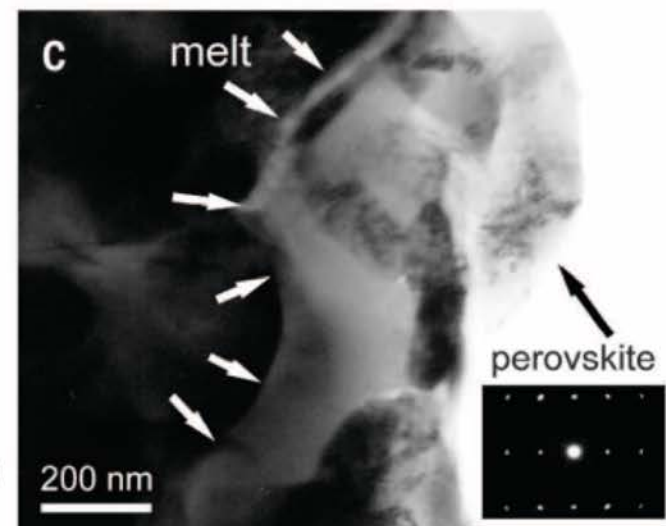
Laser Heated DAC Exp. Rw



IR analyses in the heat spot

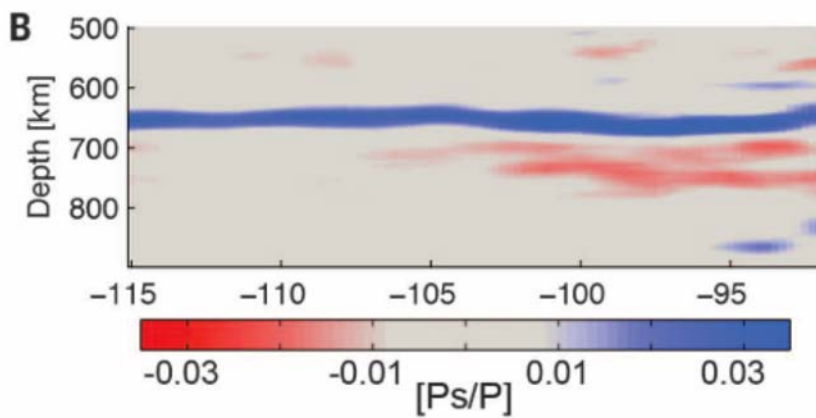
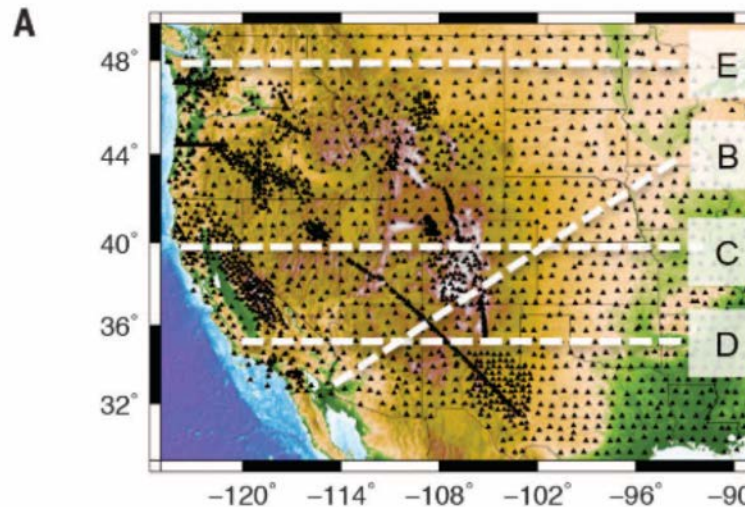


TEM analyses on recovered samples



Schmandt et al., Science, 2014

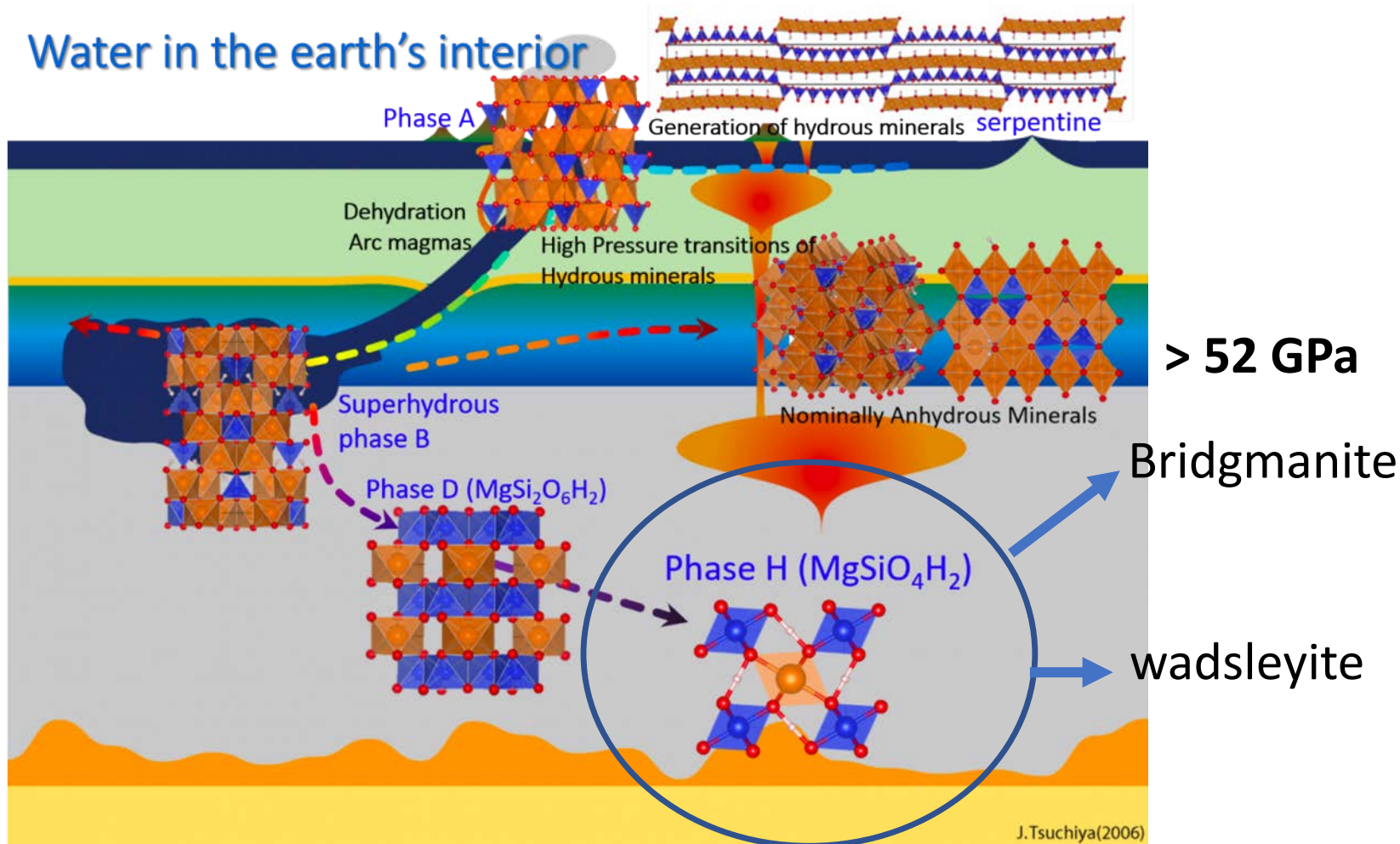
Water Transport : TZ => LM



- 0.68 to 1% partial melting at the TZ/LM limit may explain the reduction of V_{Ps}

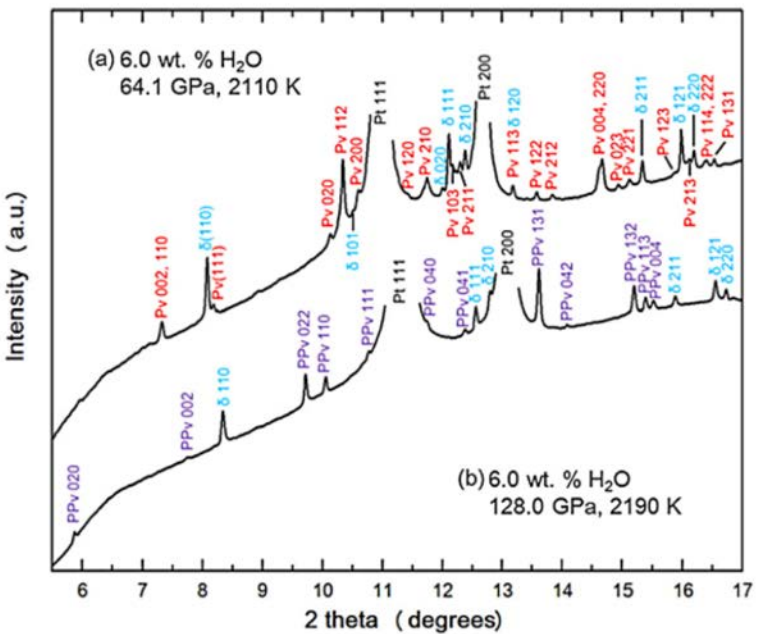
Schmandt et al., Science, 2014

Water Transport : Lower Mantle

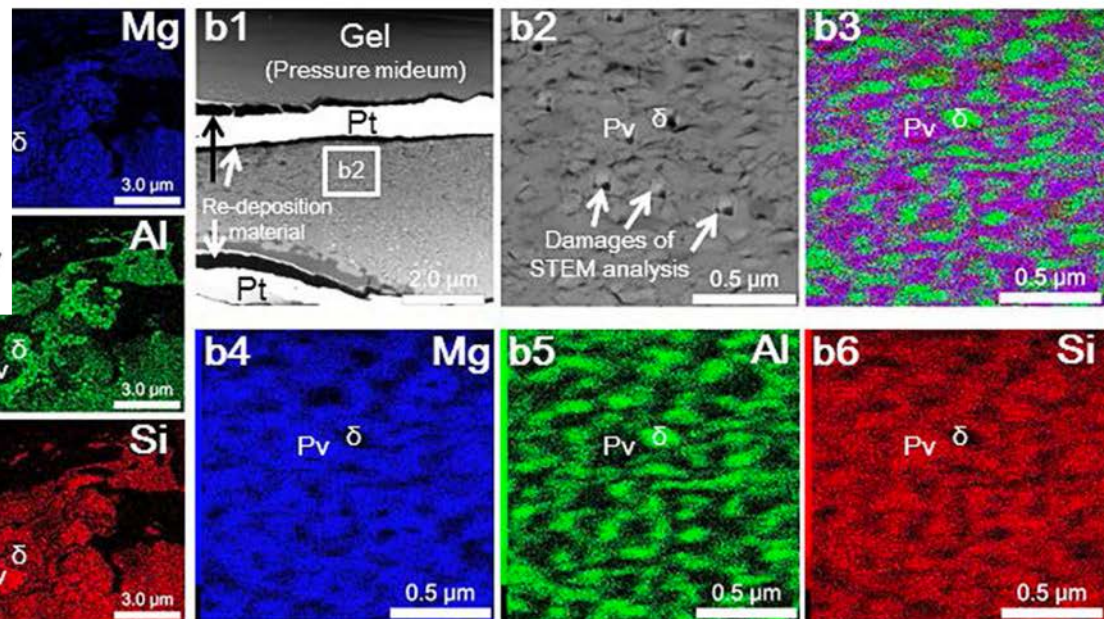


Water Transport : Lower Mantle

70 mol% MgSiO_3 – 30 mol% Al_2O_3 et 6 wt% H_2O

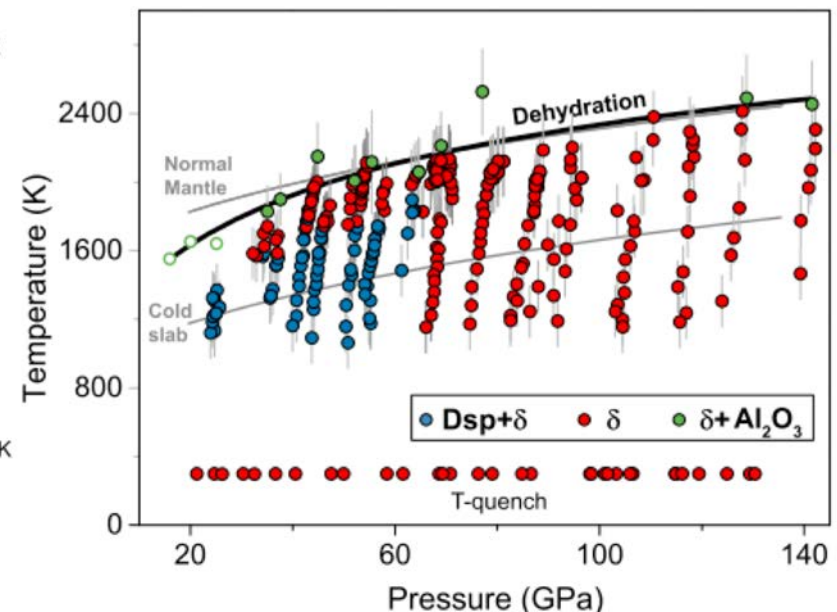
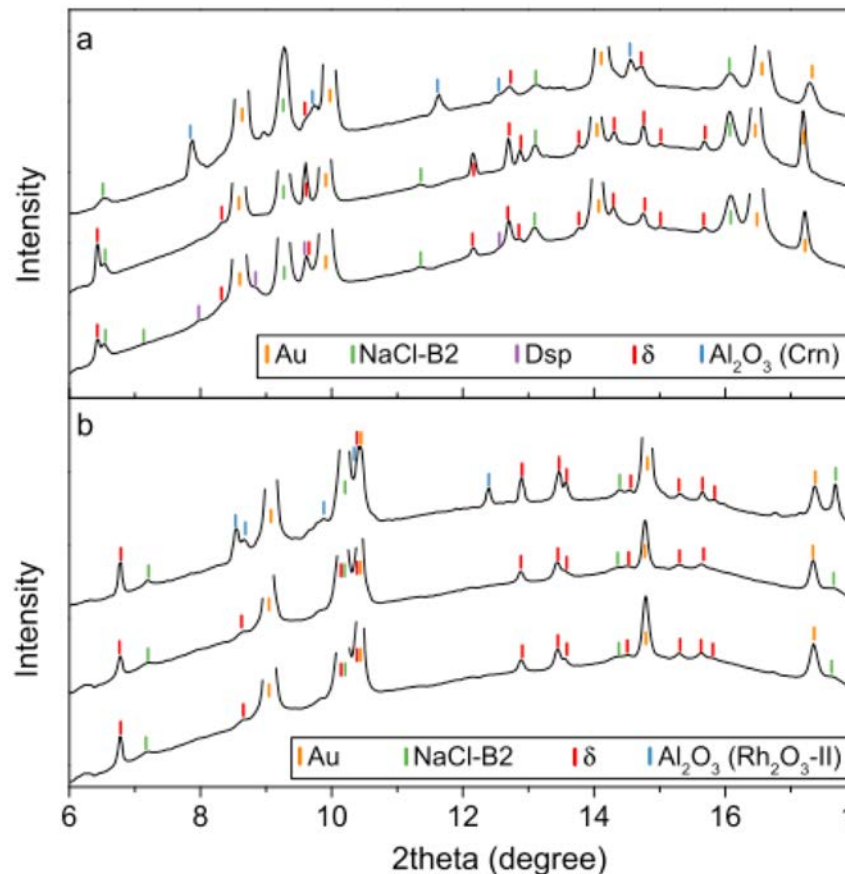


- Al in the composition stabilizes the structure



Water Transport : Lower Mantle

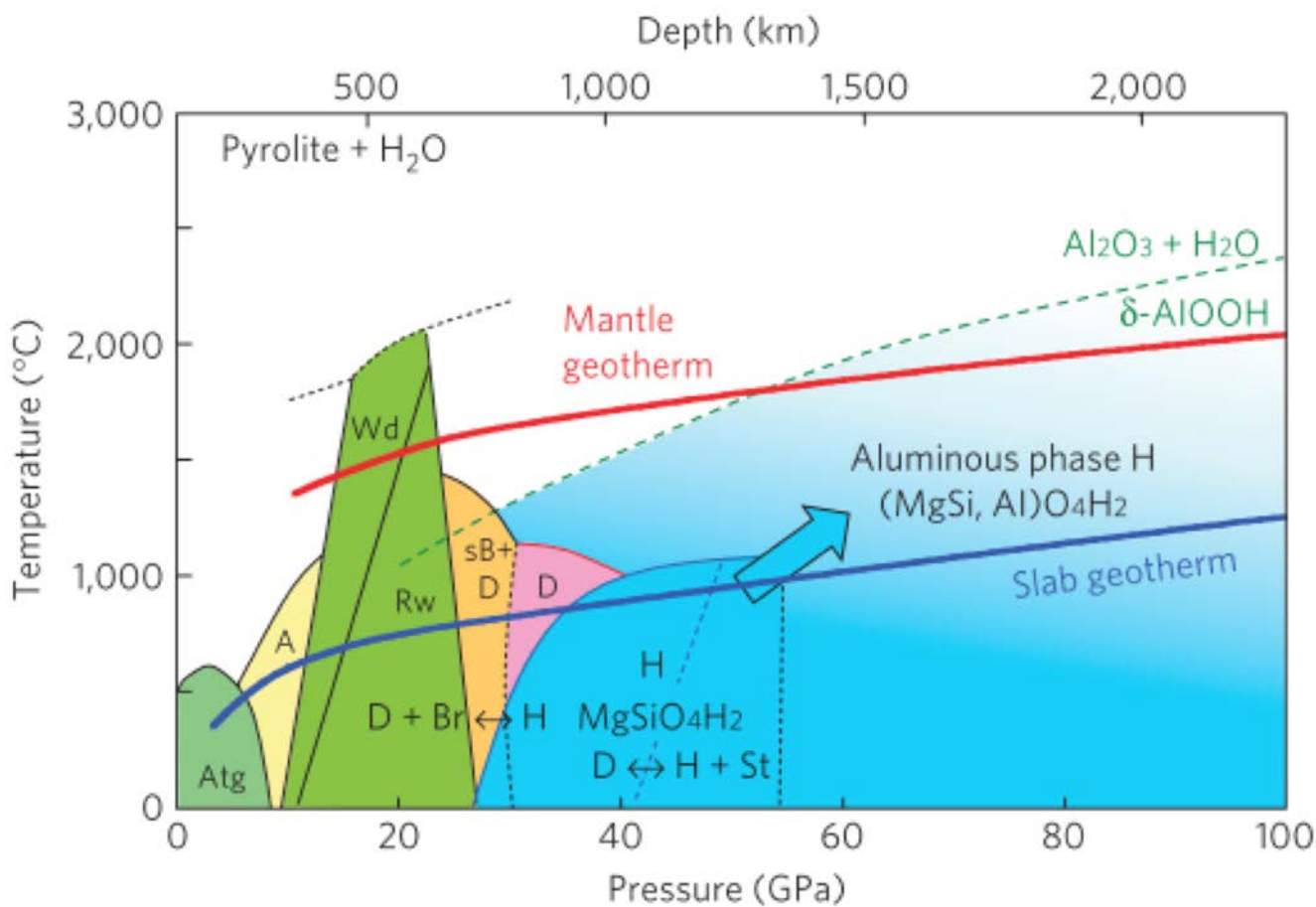
AlOOH



Brown ticks: Au; green ticks: NaCl-B2 phase; purple ticks:
diaspore; red ticks: δ -AlOOH; blue ticks: corundum or
 Rh_2O_3 -II type Al_2O_3 .

Duan et al., EPSL, 2018

Water Transport : Lower Mantle



Nishi et al., Nature Geoscience, 2014

Les Houches 2022

Water Transport : Lower Mantle

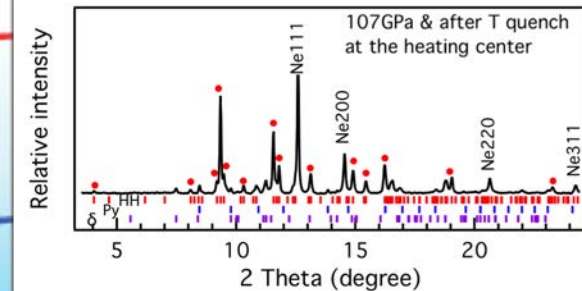
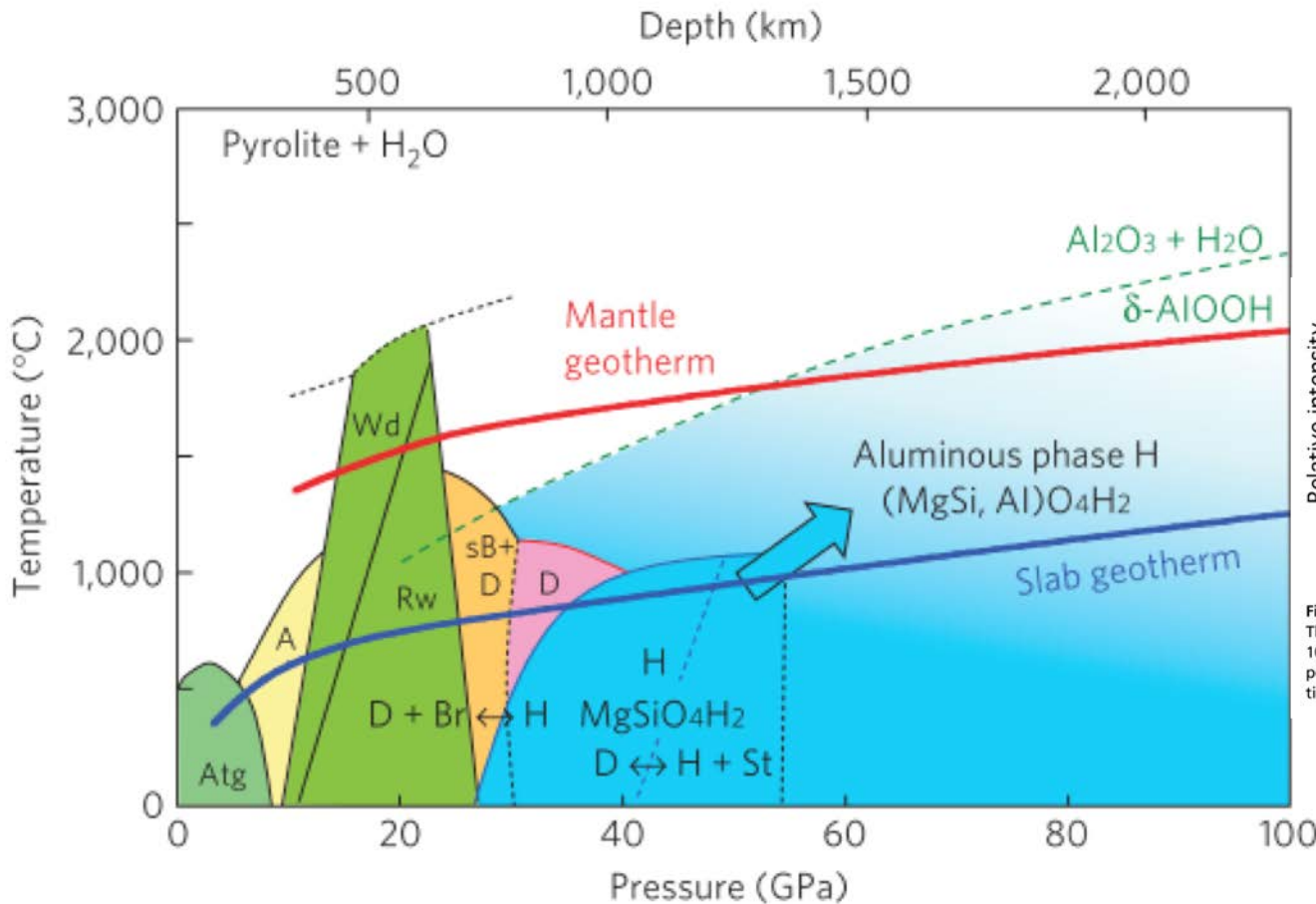


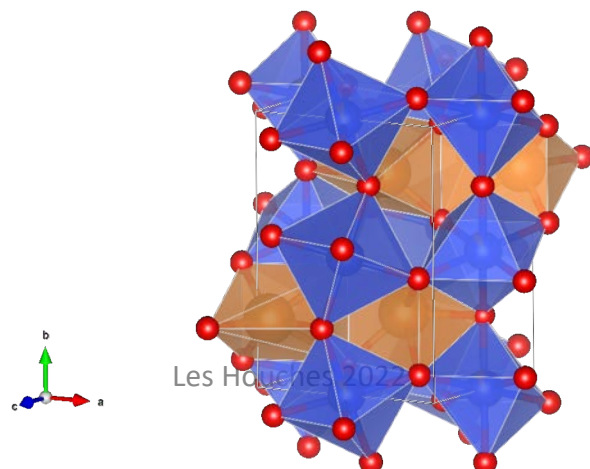
Fig. 3. Powder XRD pattern of the HH phase in A20 collected in region C. The HH phase (marked with red dots) was dominant under P - T conditions of 107.0 GPa and 2,000–2,400 K (X-ray wavelength: 0.3738 Å). The calculated peak positions of the HH phase, Py phase, and δ -phase are indicated by small ticks, showing coexistence of small amount of both P-phase and δ -phase.

Nishi et al., Nature Geoscience, 2014

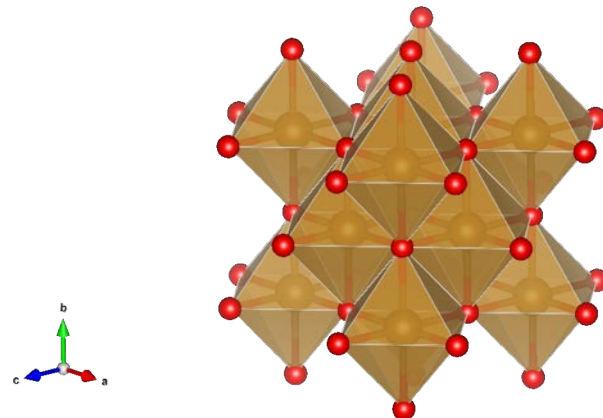
Les Houches 2022

Homogenous Lower Mantle?

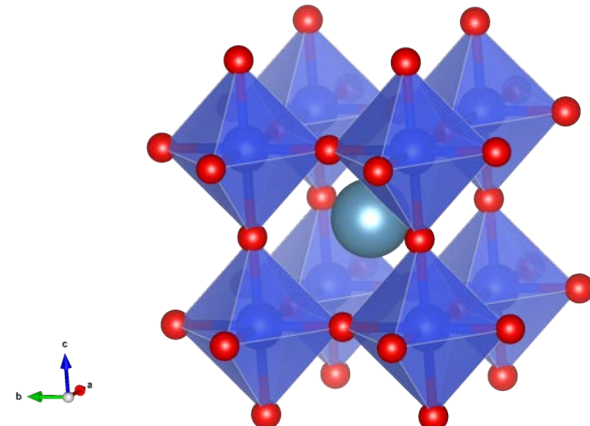
Bridgmanite $(\text{Mg},\text{Fe})\text{SiO}_3$



Ferropericlase $(\text{Mg},\text{Fe})\text{O}$

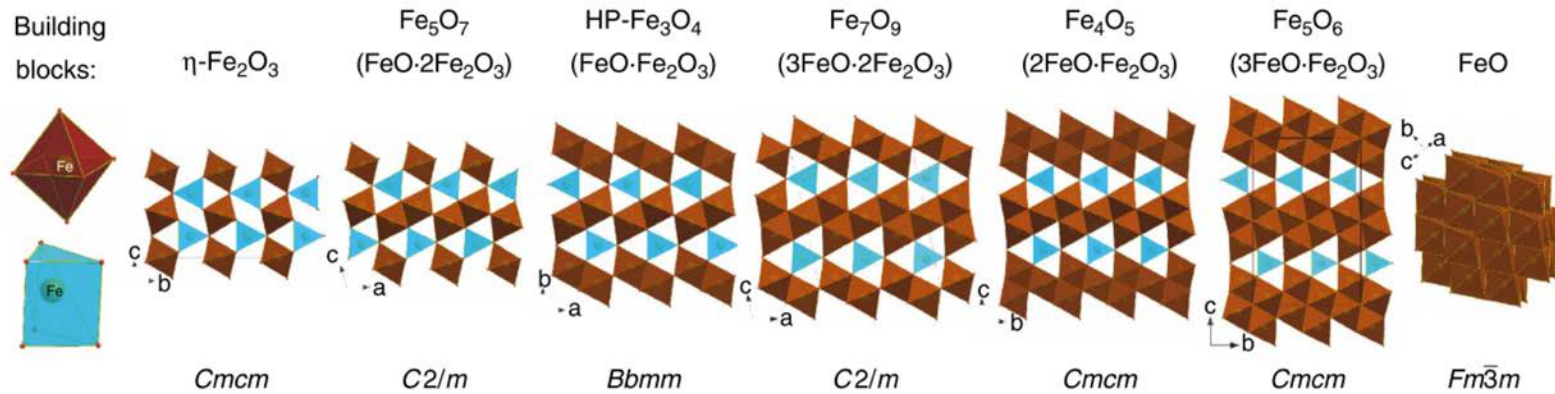


Davemaoite CaSiO_3



Les Houches 2022

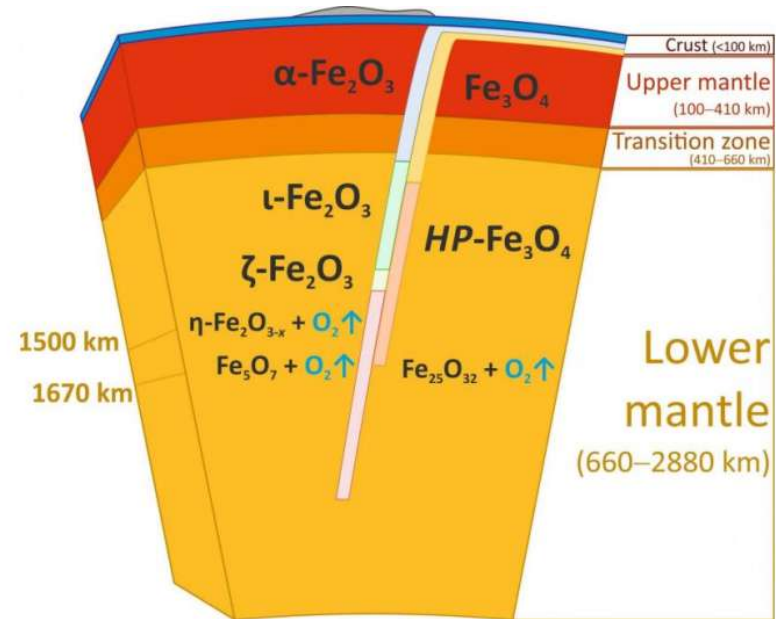
New Iron Oxides



Bykova et al., Nat. Com., 2016

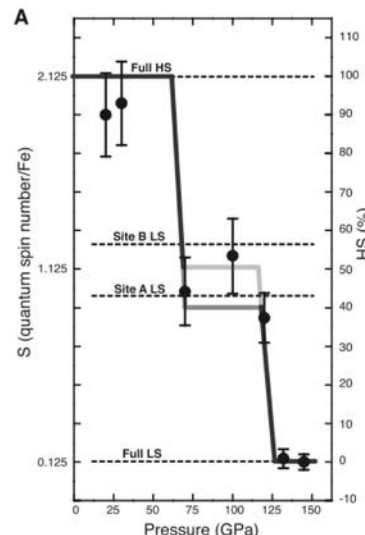
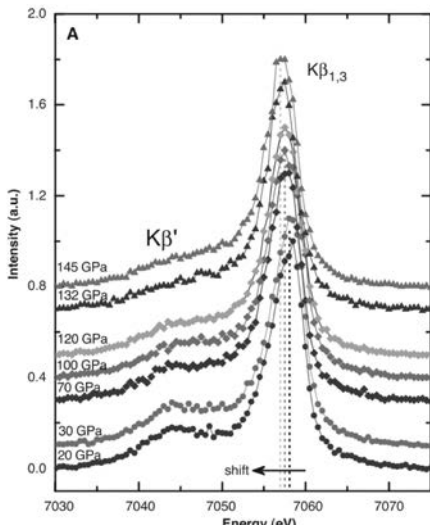


Les Houch

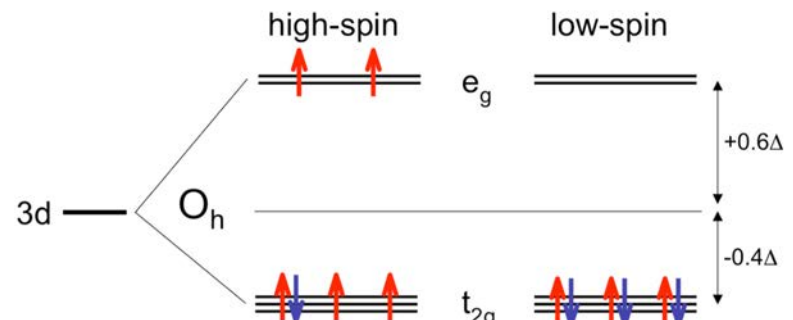


Iron Spin Transition

$(\text{Fe}, \text{Mg})\text{SiO}_3$

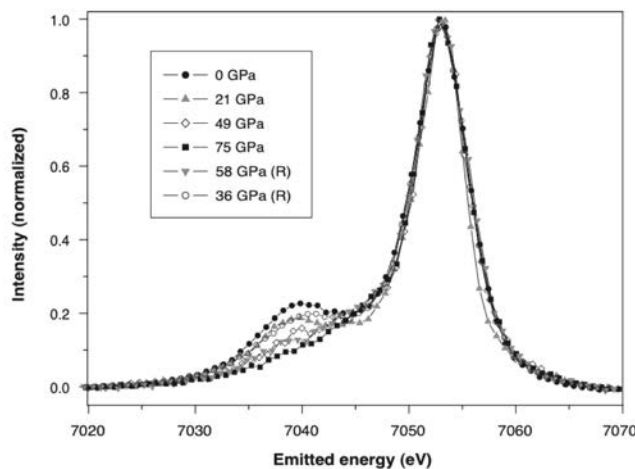


Pressure induced iron spin transition



X-ray Emission Spectroscopy through DAC

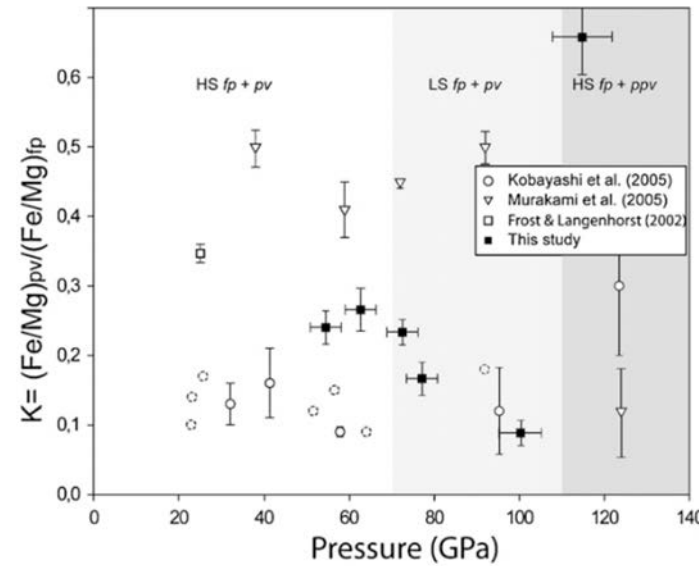
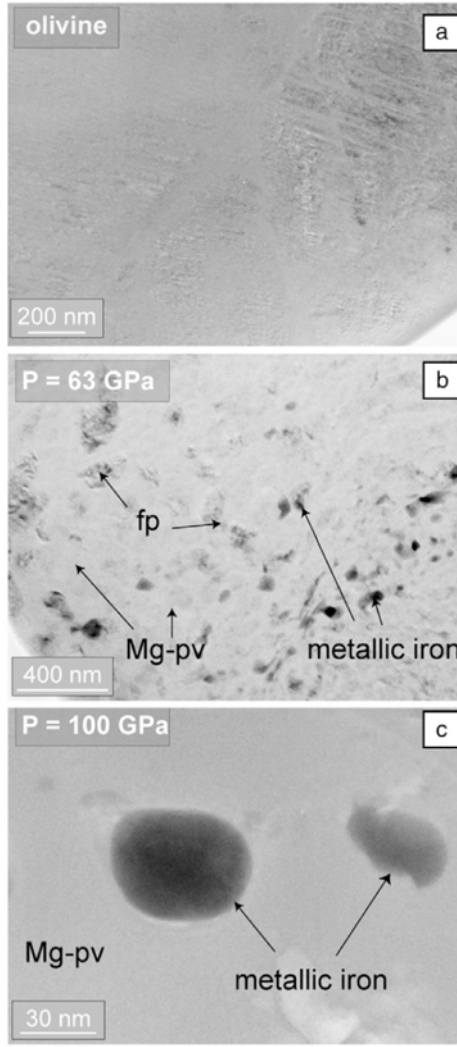
$(\text{Fe}, \text{Mg})\text{O}$



Badro et al., Science 2003

Badro et al., Science 2004

Iron Spin Transition

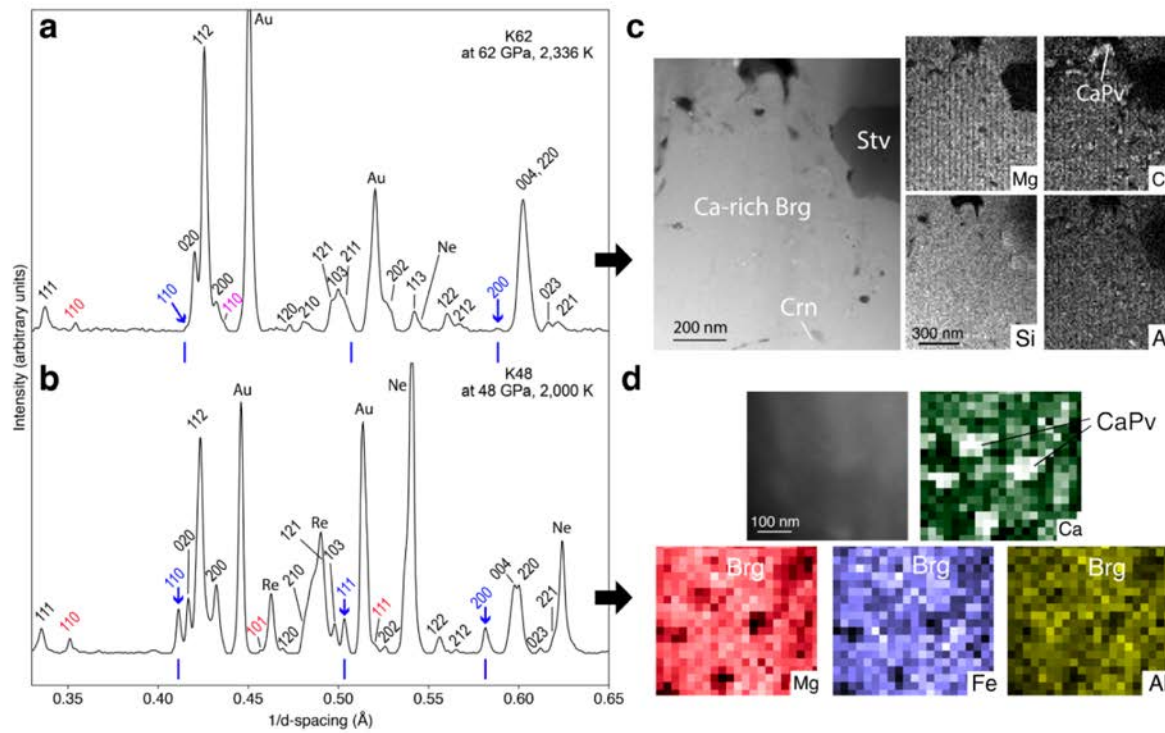


Auzende et al., EPSL 2008

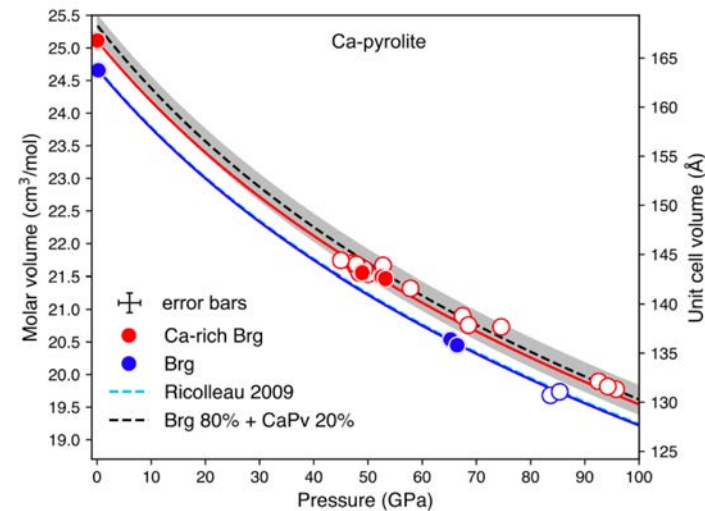
- Change in the Iron Partitioning Coefficient
- Increase the thermal conductivity

Double Perov. To Single Perov.

Laser Heated DAC exp. on :
Ca-enriched pyrolytic, Komatiitic, $\text{Ca}_{0.1}\text{Mg}_{0.8}\text{Fe}_{0.1}\text{SiO}_3$

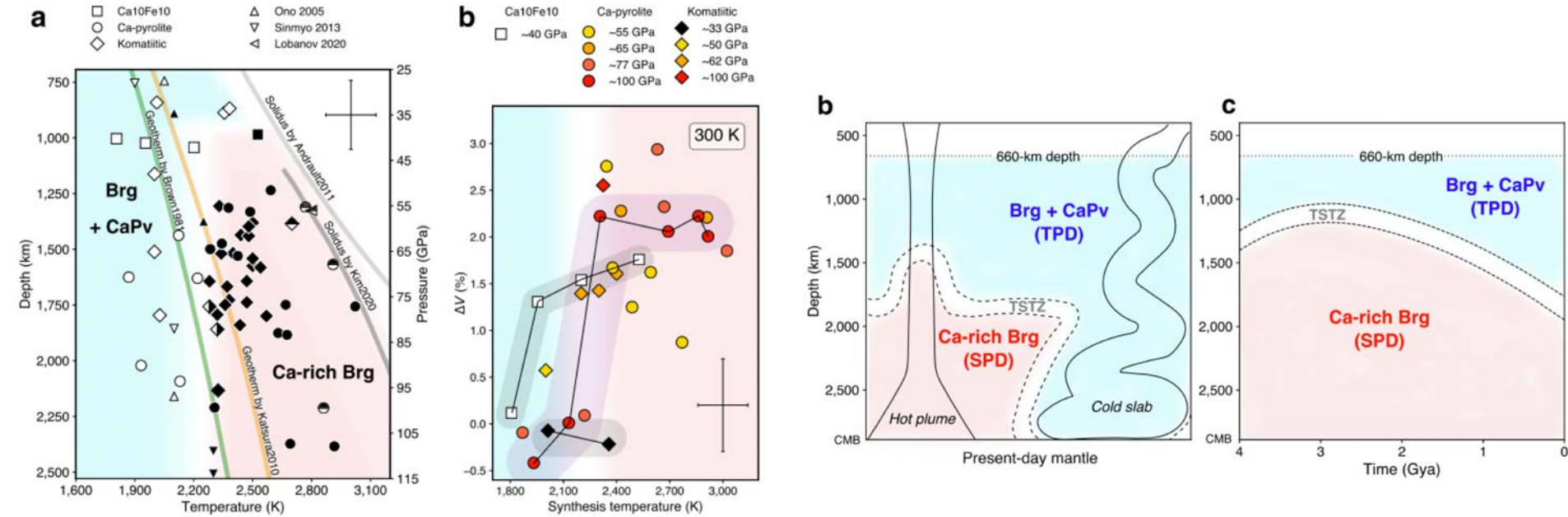


Ca-rich bridgemanite (Brg), CaSiO_3 perovskite (CaPv), stishovite (St), and corundum (Crn)

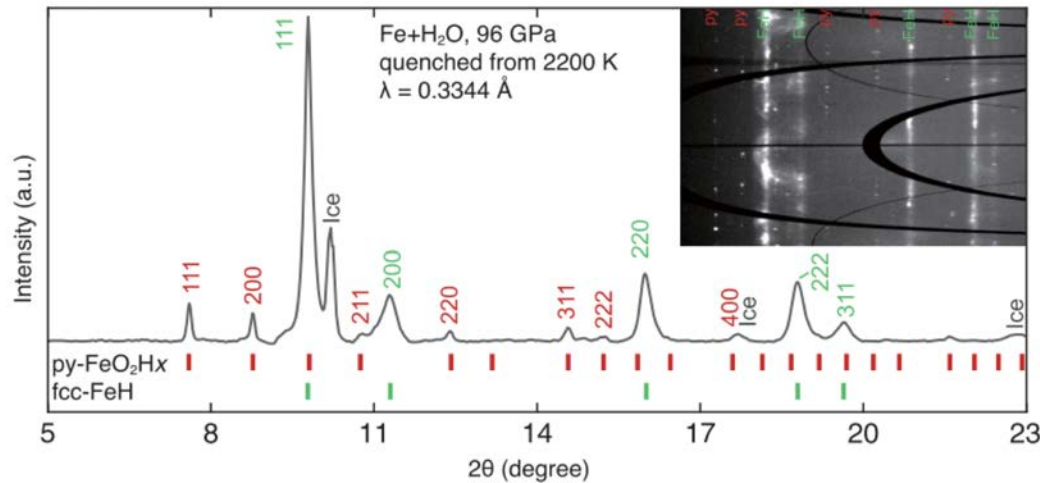


Calcium Dissolution into
Bridgemanite with Temperature

Double Perov. To Single Perov.

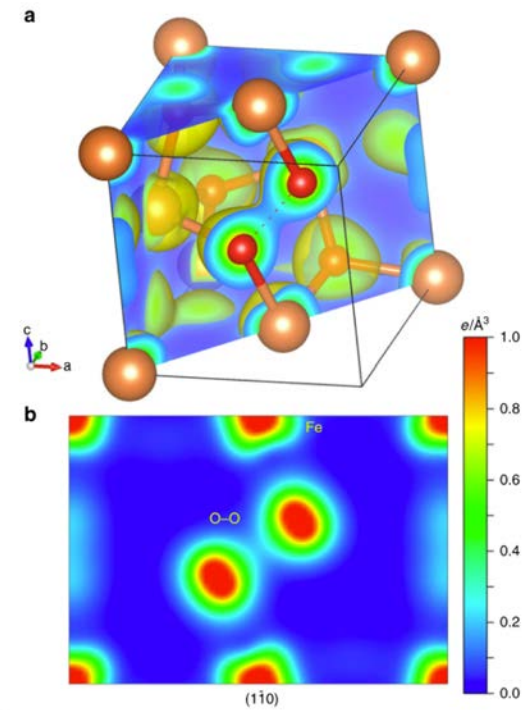


New Oxygen Valence



Mao et al., NSR 2018

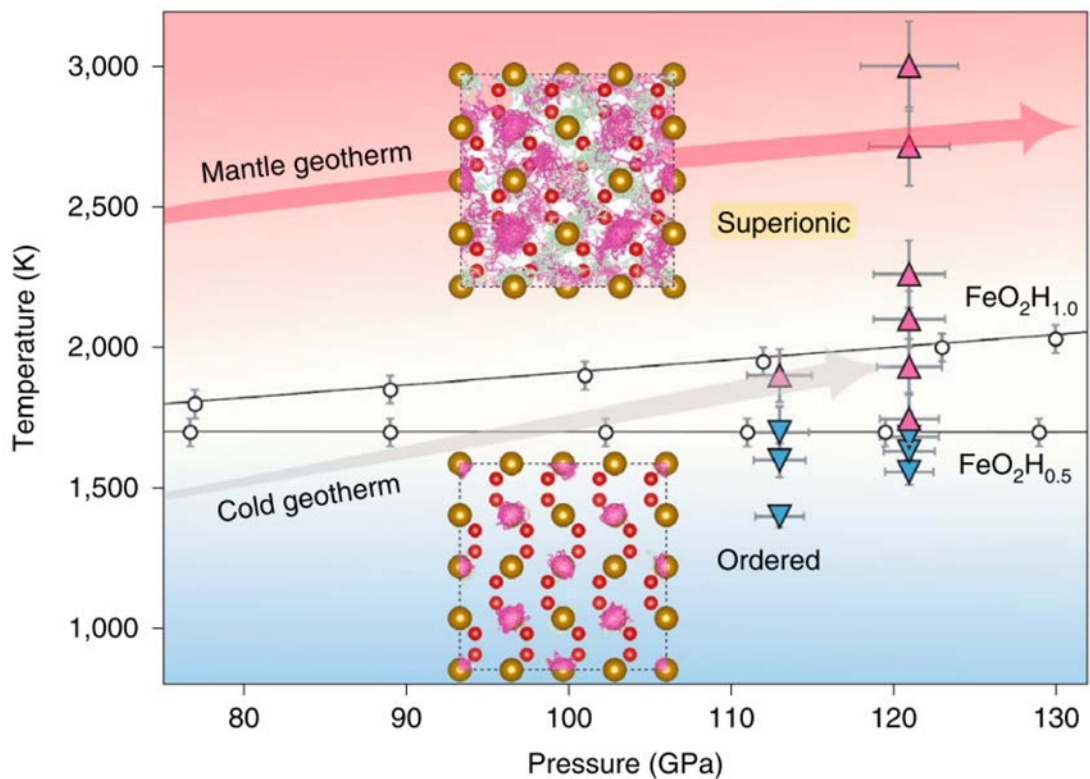
Hu et al., Nature 2016



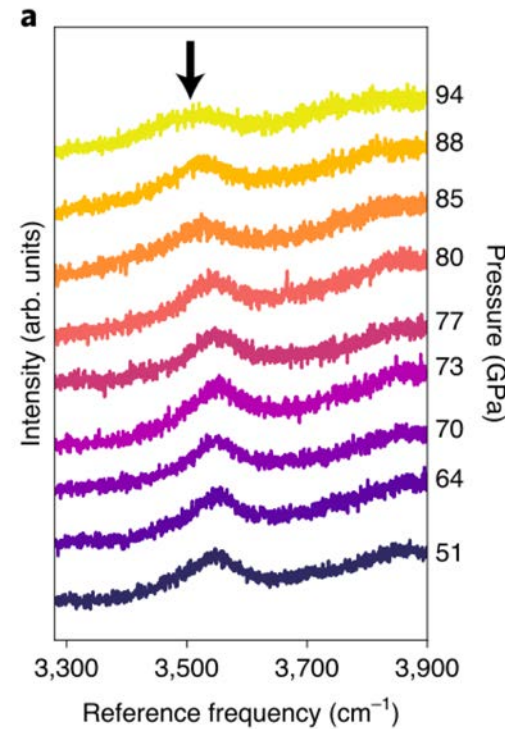
Liu et al., Nature Com. 2017

- #### ➤ Peroxide-bearing Phase FeO_2H_x : change in oxygen valence

Superionic Hydrogen



Raman spectroscopy



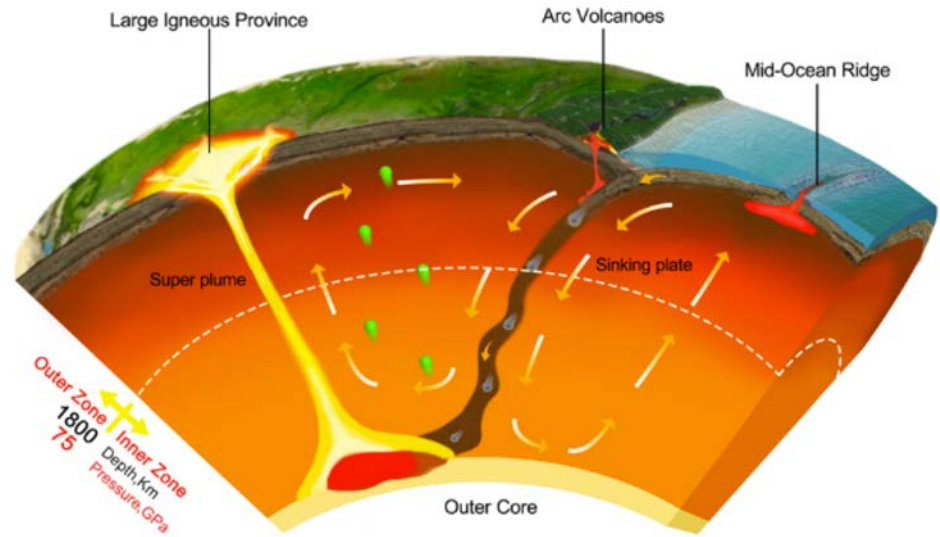
Hou et al., Nature Geosci. 2021

Highly diffusive hydrogen => Modifies transport mechanisms for charge and mass:
-electrical conductivity, magnetism, redox, hydrogen circulation and hydrogen isotopic mixing in Earth's deep

Homogenous Lower Mantle?

At about 1800 km :

- New iron oxide stoichiometries : release of O
- Pressure enhances and changes the electronic configuration of 3d electrons : thermal conductivity and iron partitioning of minerals
- Two Perovskites to Single Perovskite Transition
- Stoichiometry of minerals being based on the ionic valences of Na^+ , Mg^{2+} , Fe^{2+} , Fe^{3+} , Al^{3+} , Cl^- , O^{2-} , etc. is no longer a constraint
- Superionic hydrogen at high P-T
- Oxygen valence of -1



Mao and Mao, Matter Radiat. Extremes, 2020